An Energy Balance Model of Titan's Hydroclimate

Nicholas James Archambault

Department of Physics
Yale University
19 May 2021

Faculty Advisor: Juan M. Lora, Department of Earth and Planetary Sciences

Abstract

Titan is the solar system's second largest moon, a world both familiar and eerily alien, where a hazy atmosphere conceals a surface topography of hydrocarbon dunes and methane rivers and seas. Frequently described as the solar system body most analogous to Earth, it is the destination of NASA's Dragonfly mission, scheduled to arrive in 2034, which will deploy a rotorcraft to analyze samples of complex atmospheric chemistry and varied surface composition.

In this senior capstone project for the Department of Physics, we construct an energy balance model (EBM) to simulate and investigate Titan's climate, specifically the mechanisms driving global energy and moisture transport. Titan is the only other world in the solar system to feature an active hydrological cycle, a process of constant interaction between the atmosphere, surface and subsurface that circulates and replenishes liquid methane through processes of evaporation and precipitation. One of Titan's most intriguing unexplained features is the confinement of all filled lake and sea basins to latitudes poleward of 55 degrees. Such distribution, which leaves equatorial and mid latitudes arid, implies pole-to-pole transport of moisture governed by seasonal and orbital cycles. Given the polar concentration of surface liquid, Titan's global relative humidity is much greater at high latitudes than low, in an inversion of the humidity profile observed on Earth.

This paper realizes a one-dimensional model of the latitudinal dependence of energetic and hydrological processes, allowing the sensitivity of their parameters to be explored at low computational costs. The model is calibrated on known climatological results for energy distribution on Earth, then applied to Titan and adjusted to understand the influence of certain free parameters whose true values are unknown. By numerically integrating differential equations that evaluate moist static energy flux and its relationship to solar heating, the Titan version accurately replicates known temperature, energy, and moisture profiles. Implementing a recursive feedback function, we show that the model permits the natural emergence of a convergent solution for the relative humidity profile, matching that observed by data. The sensitivity of this profile is also analyzed, and the physical processes behind its response explored. By illuminating the intuition behind the planetary constraints governing moisture distribution, the model provides a flexible, accessible starting point for further investigation of Titan's energetic processes.

Contents

1 Titan as a System **6**
- 1.1 History . . . 6
- 1.2 Atmosphere . . . 8
  - 1.2.1 Structure . . . 8
  - 1.2.2 Composition . . . 8
  - 1.2.3 Haze . . . 10
- 1.3 Surface . . . 11
  - 1.3.1 Plains . . . 12
  - 1.3.2 Dunes . . . 12
  - 1.3.3 Hummocky Terrain . . . 14
  - 1.3.4 Labyrinth . . . 15
  - 1.3.5 Craters . . . 15
  - 1.3.6 Lakes and Seas . . . 16
- 1.4 Methane Cycle . . . 17

2 Theory **20**
- 2.1 Motivation . . . 20
- 2.2 Meteorological and Physical Background . . . 22

3 Model **28**
- 3.1 EBM . . . 28
- 3.2 Hydrological Function . . . 30

4 Results **35**
- 4.1 Sensitivity Tests . . . 35
  - 4.1.1 Sigma . . . 37
  - 4.1.2 Lambda . . . 39
  - 4.1.3 Diffusivity . . . 39
  - 4.1.4 Relative Humidity . . . 42
- 4.2 Recursive Relative Humidity Function . . . 45

5 Discussion **48**

List of Tables

1.1 Percentages of total surface area on Titan covered by major geomorphological units. Sourced from *Lopes et al, 2020* [30]. 11

3.1 Parameters and constants for Earth and Titan, with units and descriptions. Parameters whose values for Titan were later expressed and tuned by model outputs are left blank. 29

4.1 Baseline estimations of parameters whose true values are unknown for Titan. 35
4.2 Best estimates for terms of relative humidity profiles that produce meaningful model results. 45

List of Figures

1.1 An aerial view of rugged terrain as the Huygens probe descended to the surface of Titan. In the foreground, the dark homogeneous area is a combination of hydrocarbons that have never been recreated in any laboratory. In the upper middle, dark branching features are river valleys carved by surface methane runoff. Image source: NASA. 7
1.2 The structure of Titan's and Earth's atmospheres plotted as (a) logarithmic pressure versus temperature and (b) altitude versus temperature. These diagrams demonstrate that despite the thickness and coldness of Titan's, the two atmospheres are structurally similar. Sourced from *Roe, 2015* [15]. . 9
1.3 Orbital characteristics of Titan over the past million years. The variance observed in these parameters drives Milankovitch-like cycles, which contribute to asymmetric polar moisture transport and pole-to-pole methane distribution. 18

2.1 The interactions of basic processes in the climate system. Sourced from *Mechoso et al., 2015* [92]. 21
2.2 Insolation strikes the Earth's surface at different angles depending on latitude. Solar energy is more concentrated near the equator, where it irradiates the surface perpendicularly. At the mid latitudes and poles, however, the same cross-sectional profile of sunlight is diffused across a greater areal extent due to the angle at which it strikes, leading to less concentration and warming. 23
2.3 Earth's Hadley cell draws warm, dry air along the surface from the high pressure subtropics to the low pressure equator, where it dumps precipitation within the ITCZ before rising, expanding, and being pushed back to the subtropics at high altitudes. 25

3.1 The linearization of the Stefan-Boltzmann law of emittance for Earth and Titan. Earth's temperature range runs from 280 to 295 K for a true surface temperature of 288 K and an equilibrium temperature of 258 K. Titan's temperature range runs from 88 to 98 K for a true surface temperature of approximately 92.5 K and an atmospheric offset of 7.5 K. 30
3.2 Curve-fitting for the pressure-temperature vaporization curves of water vapor on Earth and methane on Titan over relevant planetary temperature ranges. 32
3.3 Hydrological results for Earth by latitude. 33

4.1 Hydrological results for Titan by latitude, with default parameters shown in Table 4.1, including a globally constant relative humidity. Note the differences and similarities with Earth's defaults. Temperature (4.1a) and moist static energy (4.1c) peak at the equator, albeit at different scales, and net precipitation (4.1d) reflects observed moisture-rich poles. 36

4.2 The weighting function $w(x)$, plotted for different values of σ beween 0.3 and 0.9. The black line represents $\sigma = 0.6$, considered the best estimation for the true value. Dotted vertical lines mark the latitudinal boundary where Hadley cell effects governing moisture transport should taper off as the influence of polar eddies dominates. 37
4.3 Hydrological outputs for sensitivity tests of σ. Only latent heat flux (4.3b) and net precipitation (4.3d) appear to be affected by changes to the Hadley cell extent. At higher σ values, we observe suppressed and poleward-trending peaks in latent flux, as well as less-pronounced extremes in both sub-tropical surface drying and polar surface wetting. 38
4.4 Hydrological outputs for sensitivity tests of λ. We find that higher values lead to more Earth-like profiles of latent heat flux and net precipitation across the equatorial latitudes. The profile of latent heat flux (4.4b) is more in line with GCM simulations at lower values of λ, suggesting that 1.06 is not a great approximation. These lower values, however, are more likely to result in net equatorial wetting, as shown by the blue curve in (4.4d), an unrealistic phenomenon on Titan. Further exploration and more sensitive testing would be required to balance these competing effects. 40
4.5 Hydrological outputs for sensitivity tests of D, the diffusion coefficient. The temperature (4.5a) and moist static energy (4.5c) curves produced by different values of D serve as helpful constraints in understanding the parameter's true scale. The D that produces the most appropriate temperature and moist static energy curves is on the order of 10^3, confirming that the *Williams & Kasting, 1997* approximation on the order of 10^8 was far too high. 41
4.6 The range of simulations approximating Titan's relative humidity profile, represented by the green area, as conducted in *Lora & Ádámkovics, 2017* [95]. 42
4.7 Hydrological outputs for all 78 feasible expressions for relative humidity that were initially tested. Broad trends can be observed from these plots, namely that although all expressions conform to Titan's known relative humidity profile, only some of them produce meaningful outputs when incorporated into the model. 43
4.8 Hydrological outputs from the four expressions that most closely match the known relative humidity profile in terms of polar behavior. We find that the variance in parameters of these functions is minute, as shown in Table 4.2, confirming the model's sensitivity to relative humidity input. 44
4.9 Relative humidity profiles generated by the recursive function for different initial conditions where δ equals 1 and the convergence threshold equals 0.01. 46

Chapter 1

Titan as a System

With complex pre-biotic atmospheric chemistry and a surface topography that is at once familiar and alien, Titan is a unique world in our solar system. It is the second-largest natural satellite, the only moon with a thick atmosphere and active weather cycle, and the only other body besides Earth with stable, standing surface liquids. Observations have revealed that Titan's organic atmospheric haze contains oxygen-bearing molecules and facilitates chemical processes unlike those found anywhere in the solar system, rendering the moon a fascinating natural laboratory for astrobiologists to study the prevalence and diversity of potential life in the universe [1]. Over its 13-year lifespan, the joint NASA and European Space Agency (ESA) Cassini-Huygens mission to the Saturnian system collected a trove of information on Titan's climate, chemical and surface composition, and seasonality that has allowed researchers to better understand the moon as a system. NASA's Dragonfly mission, scheduled to launch in 2026 or 2027 and arrive at Titan in 2034, will deploy a rotorcraft to dozens of locations across the surface in an effort to build upon the preliminary findings of Cassini-Huygens, marking the first time a flying craft will transport its payload for repeated, targeted experimentation on an extraterrestrial world [2].

Besides investigating Titan's chemical and climatic history, Dragonfly will provide insights crucial to understanding Earth's own development as a planet. Titan's thick atmosphere, dominated by nitrogen, and its intimately intertwined surface-atmosphere interaction make it an analogue to a very early Earth, with a distinctive methane-based hydrological cycle that acts as an extreme version of Earth's water cycle. Despite Titan's radically different composition, there is perhaps nowhere in the solar system that so closely resembles Earth. The moon features comparable surface pressure, temperature, and gravitational effects, as well as broad deserts of arid dunes at low latitudes, stable lakes and seas of liquids at high latitudes, and a network of fluvial, pluvial and aeolian processes that transport materials across the surface. Meteorological patterns of circulation appear to mirror cycles of moisture distribution found in Earth's atmosphere.

In this chapter, we review Titan's observational history and its defining orbital, atmospheric, and geomorphological characteristics, providing a framework within which to realize a surface-atmosphere energy balance model and investigate the question of asymmetrical moisture transport.

1.1 History

Titan is the largest moon of Saturn, which orbits the Sun at an average distance of about 1.4 billion km, ten times the orbital distance of Earth. During its orbital period of 15.95 Earth days, Titan stays tidally locked, meaning it always shows the same face to Saturn. With a radius of roughly 2,575 km, Titan is larger than Mercury and around 40% the size

of Earth.

Titan was first observed by Dutch astronomer Christiaan Huygens in 1655, and the existence of its atmosphere was confirmed in 1944 by Gerard Kuiper, who posed the first estimations of Titan's atmospheric stability based on spectral observation of methane [3]. Preliminary ground-based analyses of temperature range constraints and the presence of nitrogen were conducted throughout the 1970's by *Morrison et al., 1972* and *Lewis, 1971* [1]. Photographs taken by Voyager I and Voyager II during their flybys of Titan in the 1980's revealed little more than a hazy orange ball, but spectral data and radio-wave probing of the atmosphere facilitated a number of key insights, namely the confirmation of substantial atmospheric nitrogen [4], a surface temperature of 92–93 K [5], and a surface pressure of approximately 1.5 times that of Earth [6].

New findings were illuminated by the landmark 1997 Cassini-Huygens mission. As it collected a cache of data on Saturn, Cassini conducted 127 flybys of Titan and made a number of scientific advances, using radar to penetrate the opaque atmosphere and map the features of nearly half of the moon's surface [7]. The most profound findings included confirmation and bathymetric measurement of surface lakes and seas composed of liquid methane; observation of the distribution of geological attributes; and the collection of evidence from rotational dynamics that supports the existence of a subsurface ocean of liquid water and ammonia [7]. In 2005, the Cassini orbiter released a small probe, Huygens, which parachuted through Titan's atmosphere to measure its composition and return photographic evidence of a rugged surface topography bearing signs of past fluvial flow. Data returned from the probe's 2.5-hour journey to the surface helped scientists formulate a more thorough understanding of the atmosphere's vertical stratification and temperature profile, informing fresh theories of atmospheric dynamics and origin [8]. The Cassini-Huygens mission is considered an unequivocal success, revealing mysteries and novel insights that have inspired and defined the next generation of Titan studies.

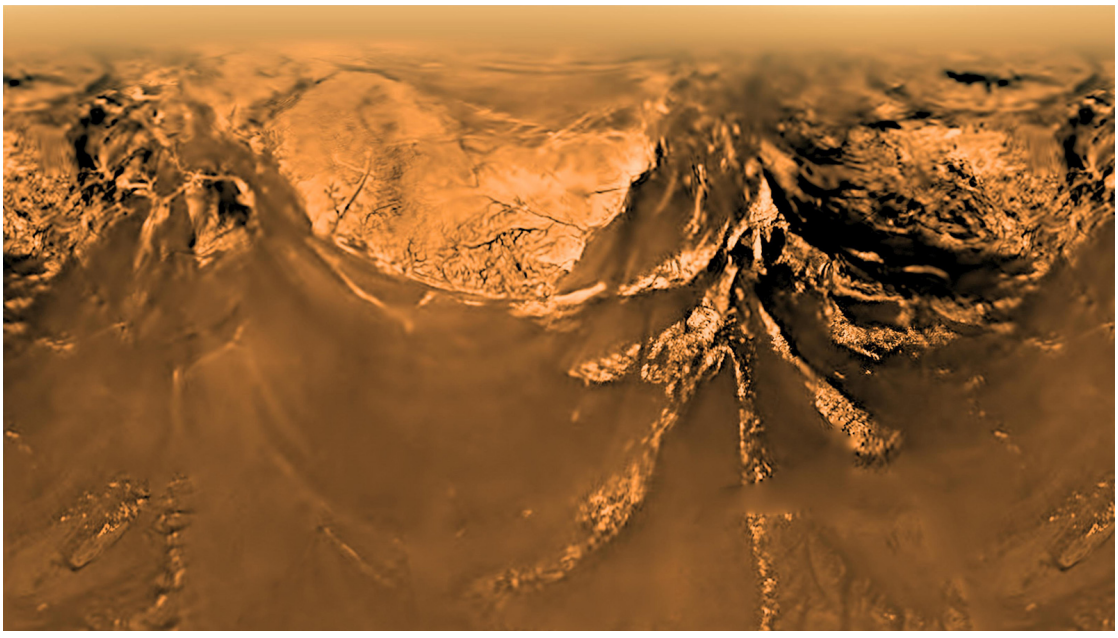

Figure 1.1: An aerial view of rugged terrain as the Huygens probe descended to the surface of Titan. In the foreground, the dark homogeneous area is a combination of hydrocarbons that have never been recreated in any laboratory. In the upper middle, dark branching features are river valleys carved by surface methane runoff. Image source: NASA.

1.2 Atmosphere

Titan is shrouded by a thick, dense atmosphere that exhibits a stratified structure akin to that of Earth's, with layers defined by their temperature profiles, vertical extents, and chemistry. The lower atmosphere is composed of approximately 98.5% nitrogen (N_2) and 1.5% methane (CH_4) [9], while the upper layers contain trace amounts of a number of diverse molecules and hydrocarbons, including ethane (C_2H_6), acetylene (C_2H_2), ethylene (C_2H_4), propane (C_3H_8), and benzene (C_6H_6), among others [10, 11]. Many of these molecules were first detected by Voyager and by ground-based observation, before Cassini-Huygens' arsenal of in-situ and remote sensing instruments permitted further analysis. Agglomerated measurements have identified over 20 constituent molecules, most notably noble gases and isotopes — both of which are crucial to understanding atmospheric evolution [1] — and a collection of nitrogen-dependent molecules [12]. These findings have underscored the important role nitrogen plays in atmospheric chemistry; they also revealed that the general pre-Cassini conception of Titan's chemical processes vastly underestimated the activity and complexity of the upper atmosphere [1]. Measurement by Cassini-Huygens has also led to a robust understanding of physical atmospheric structure and its relationship with atmospheric chemistry and surface processes.

1.2.1 Structure

Titan's atmosphere is comparable to Earth's, with a clearly defined troposphere, stratosphere, mesosphere and thermosphere [13]. However, orbiting at a distance from the Sun ten times that of Earth, Titan receives only 1% of the incoming insolation that Earth does. At 1.35 ms^{-2}, the acceleration due to gravity on Titan is relatively weak, just 14% the acceleration found on Earth. *Scale height*, a common metric by which to evaluate a planetary atmosphere, is dependent upon gravitational influence and atmospheric composition, and defined as the altitude at which planetary surface pressure decreases by a factor of $\frac{1}{e}$, or 2.718^{-1}. Less gravitational restraint allows Titan's atmosphere to extend further away from the surface, reaching scale heights of 15 to 50 km as compared to 5 to 8 km on Earth [14].

The height of the atmosphere and the presence of large particulate aerosols impede most of the already-weak incoming solar flux: only 11% of sunlight at the top of the atmosphere penetrates through to Titan's surface, as opposed to nearly 57% on Earth [16]. Consequently, Titan's average surface temperature is a frigid 92 K [5, 13], and surface pressure hovers around 1.5×10^4 Pa. These values lie near the triple point temperature and pressure conditions for methane, allowing it to exist both in gaseous and liquid form [1, 13].

1.2.2 Composition

As previously noted, Titan is a hydrocarbon world, despite its atmospheric prevalence of N_2. Over twenty different molecules have been observed over the course of decades by both Voyager crafts, ground-based measurements, remote sensing by the Cassini orbiter, and in-situ analysis by the Huygens probe. Under various atmospheric conditions, these known molecules include not just hydrocarbon compounds like methane and ethane but also carbon monoxide and dioxide, ammonia, and water vapor.

Vertical abundances of these molecules have been shown to increase with altitude, a common feature for molecules that are catalyzed by interaction with sunlight in the outer layers of the atmosphere. Such findings suggest that photochemistry plays a key role in Titan's complex chemical processes and the generation of its characteristic haze [1, 13].

One major reason Titan stands out as a tantalizing destination for future exploration

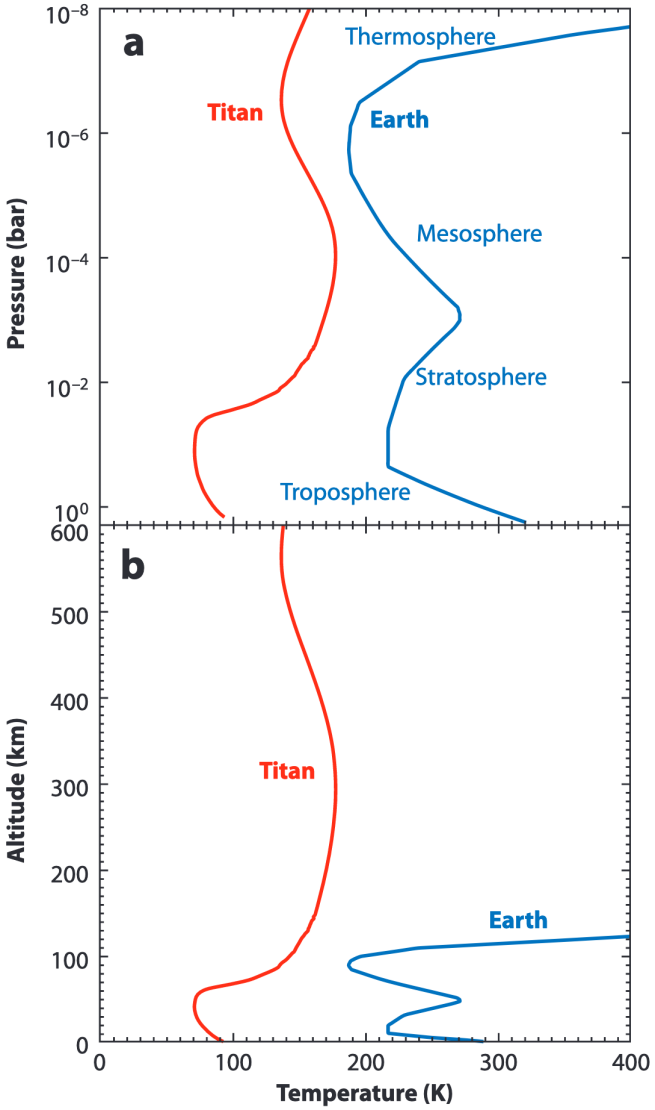

Figure 1.2: The structure of Titan's and Earth's atmospheres plotted as (a) logarithmic pressure versus temperature and (b) altitude versus temperature. These diagrams demonstrate that despite the thickness and coldness of Titan's, the two atmospheres are structurally similar. Sourced from *Roe, 2015* [15].

is this atmospheric chemistry, specifically the presence of a variety of 'CHON' compounds, which contain combinations of the four most common elements in living organisms — carbon, hydrogen, oxygen and nitrogen. Pre-Voyager photochemical models predicted the occurrence of such organic molecules as a result of methane photolysis in the upper atmosphere [17, 18, 19]; later, measurements by Cassini-Huygens confirmed their existence and provided constraints on eddy diffusion profiles of the troposphere and thermosphere [20, 21]. Eddy diffusion, or turbulent atmospheric mixing, is an essential component of a complete chemical mapping of the atmosphere that determines the duration of molecules' existence in particular atmospheric layers. The composition, insolation, and temperature of these layers affect how such molecules are destroyed or lost due to reactive processes, condensation, and photolysis [1].

At the top of Titan's atmosphere, solar photons and cosmic rays dissociate CH_4 and N_2 in chemical processes that destroy CH_4 molecules, generating H_2 and many of the other observed organics [1]. Sunlight is responsible for roughly 90% of N_2 catalysis [22]; higher-

energy photons are absorbed by N_2 toward the top of the atmosphere, while lower-energy photons are able to penetrate further before triggering methane dissociation [22]. In the stratosphere, acetylene (C_2H_2) and diacetylene (C_4H_2) absorb the lowest-energy photons not absorbed by methane to form radicals, or highly reactive molecules with an unpaired electron. These radicals subsequently catalyze methane, providing an alternative source of methane destruction that does not involve photons or direct photolysis [23]. The replenishment of both surface and atmospheric methane, even as it is continually dissociated by various means across atmospheric layers, is an outstanding mystery of Titan's planetology.

Despite the panoply of reactive hydrocarbons, Voyager's discovery of oxygen-bearing molecules in Titan's atmosphere [24] was the impetus for sustained, deeper investigation of Titan's atmospheric phenomena. A key finding from Cassini-Huygens was confirmation of an inflowing stream of O^+ ions into Titan's upper atmosphere [25, 26]. Theoretical modeling efforts have ruled out primordial remnants or interior outgassing as sources of the carbon monoxide (CO) into which these oxygen molecules are incorporated [26], suggesting that the source is external. Water plumes venting from the poles of Enceladus, another of Saturn's moons, are theorized to supply the vast majority of neutral hydroxide (OH) in the Saturnian system [25] and account for the upper atmosphere synthesis of CO, the fourth most common molecule in Titan's atmosphere [26]. These oxygen ions are deposited at the same altitudes at which other heavy ions were previously observed by Cassini-Huygens, raising the intriguing possibility of pre-biotic molecule formation [1]. *Hörst et al., 2012* showed that laboratory attempts to replicate Titan's physical and chemical conditions permitted the formulation of amino acids and nucleobases, suggesting that similar processes may occur on Titan.

1.2.3 Haze

Images of Titan are distinguished by the moon's atmospheric blanket of opaque, orange haze, particles accumulated by a process distinct from cloud formation. The haze arises from the aggregation of aerosols, or particles suspended in air or gas, produced as a result of upper atmosphere photolysis and the destruction of CH_4 and N_2. It plays a key role in balancing radiative transfer — the process of energetic transfer across a body via the reflection, absorption, and transmission of solar energy — by cooling Titan's surface and heating its stratosphere [1].

The distribution of the aerosols which comprise the haze varies with altitude — most are concentrated at altitudes above 300 km [1]. At the very top of the atmosphere, where incoming insolation is most abundant and catalysis most common, haze aerosols grow by aggregation. Between 500 and 400 km, surface chemistry plays a greater role in particle formation, as the aerosols interact with radicals generated by lower-atmosphere chemical processes. Dynamical forces also come into play at these altitudes [27], governing aerosol morphology and, subsequently, the rate at which aerosols accumulate new material and fall to the surface. Morphology is important because cross-sectional profiles determine aerosols' absorption of radiation in the ultraviolet and visible spectra, producing different optical and chemical characteristics [1].

As it is crucial to holistically understanding Titan's climate and surface-atmosphere relationship, a subset of Titan research is devoted to studying the structure and morphology of the haze by attempting to recreate it in laboratory settings. Haze analogues are known as *tholins*, a label first utilized by *Sagan and Khare, 1979* to describe the material they had created, a sticky brown substance formed by irradiation, via ultraviolet light or electrical discharge, of some combination of atmospheric gases [28]. Today, the term 'tholin' is generally accepted to refer to any of a class of materials produced when cosmic gases are exposed to an energy source [28].

Tholin analogues are valuable, accessible tools with which to investigate Titan's haze,

but they are unable to perfectly reproduce aerosols with the properties of those found on Titan. Study of these analogues has, however, revealed that the presence of N_2, CH_4, and CO render Titan's atmosphere an ideal molecular environment for rapid haze particle generation [1]. Further work remains, most notably the study of how aerosol chemistry may change following the particles' approximately 395-year descent [29] from the mesosphere to the surface. The potential for surface catalysis is greatly reduced by the dearth of sunlight that fully penetrates the atmosphere, but aerosols are produced globally and deposited onto a vast array of surface morphologies and environments, raising the possibility of chemical alterations as they interact with surface liquids or cryovolcanic flows [1].

1.3 Surface

Until recently, failure of sensors to penetrate Titan's thick atmosphere had hindered efforts to map its surface features and study surface composition. Data from Cassini observations, however, have enabled researchers to construct a more complete picture not only of the various types of surface geological units, but also their relative ages, spatial distributions, and implications for the evolution of Titan's climate [30]. The units identified include plains, dunes, lakes, impact craters, hummocky terrain — such as mountains, ridges and mounds — and labyrinth terrain, which is characterized as elevated plateaux with high densities of cross-cutting valleys possibly dissected by erosion or primordial methane rivers [31].

Differences in albedo, or reflection of solar energy, by these units point to diverse underlying compositions; though true chemical compositions are not yet known, observation with various electromagnetic spectra has permitted a broad characterization of distinct terrain types and constraints on the latitudinal extent and dependence of each [30]. As shown in Table 1.1, the surface is dominated by plains, which account for 65% of total area. Dunes comprise 17% and hummock 14%, while lakes, labyrinth and craters all constitute less than 2% of surface area [30].

Terrain Type	**Surface Coverage (%)**
Plains	65
Dunes	17
Hummock	14
Lakes	1.5
Labyrinth	1.5
Craters	0.4

Table 1.1: Percentages of total surface area on Titan covered by major geomorphological units. Sourced from *Lopes et al, 2020* [30].

Plains dominate Titan's midlatitudes, while dunes encompass much of the equatorial region, -30 to +30 degrees latitude [30]. Surface liquids contained within lakes and seas cover just 1.5% of the surface and are almost exclusively confined to latitudes poleward of 55 degrees in both hemispheres. Of over 650 filled and empty basins [32], Ontario Lacus is the only sizeable repository of liquid at the southern pole; most other basins in that locale are empty, posited to have been paleoseas [33] filled at one point in the past. The northern pole is home to the vast majority of liquid, about 80% of which is found in Kraken, Ligeia and Punga maria (seas) [30]. Work by *Lora et al., 2014* [34], among others [33, 35], has shown that moisture oscillates between Titan's poles on 45,000-year timescales in processes similar to Earth's Milankovitch cycles, which affect the distribution of incident solar heating and the progression of climatic cycles. A key component of our work explores

how Titan's orbital parameters have shaped these cycles of pole-to-pole moisture transport during the moon's climatic evolution, as covered in chapters 2 and 3.

Atmospheric chemistry results in the formation of liquid and solid particles that are eventually dispersed over the entire surface, meaning that across all its diverse features and latitudinal variation, Titan's surface is intimately and uniquely tied to its atmosphere [1]. This relationship is confirmed by emissivity data which indicate that the primary constituents of the plains, dunes, lakes, and labyrinth terrain are atmospheric organics, while craters and hummock contain higher proportions of water ice [36, 37]. Dune formation arises at the low latitudes, in spite of occasional rainfall, due to long-term aridity and the influence of aeolian processes [30]. Relative humidity increases toward the poles, permitting the formation and maintenance of a landscape populated with hydrocarbon lakes and seas. Between these two moisture extremes, the mid latitudes are dominated by vast areas of organic plains. The geomorphological contrast among these different units and their spatial footprints indicates that processes driven by climatic, seasonal and elevational conditions substantially influence the sculpting of Titan's surface [30].

1.3.1 Plains

Plains cover the majority of Titan's surface, especially in the mid latitudes. The most common type is known as undifferentiated plains, a homogeneous area of material derived from organics, whose topographical features cannot be fully discerned [38, 30]. This terrain lacks evident fluvial features, indicating that the structure of undifferentiated plains is too porous to support networks of channels [39]. It has also been determined that plains closer to the equator have spectral profiles more similar to those of equatorial dunes, suggesting intermixing of materials between the two units due to aeolian transport [30].

Other types of plains, mostly at higher latitudes [38], have been observed, and subcategorization of the plains unit includes five additional types: bright lineated plains, bright streak-like plains, variable-featured plains, dark irregular plains, and scalloped plains [38]. 'Bright' and 'dark' describe these regions' reflectance due to backscatter, as observed by Cassini's radar. The two types of bright plains are comprised of more reflective water ice-based materials transported by hypothesized joint aeolian-fluvial processes [38]. Variable-featured plains are posited to result from the erosion of mountain and hummocky terrain [30, 38]. Dark irregular plains are low-lying areas interpreted to be dampened by liquid hydrocarbons, forming a sort of mud rather than stable lakes [30, 38, 40]. Scalloped plains are likely composed of eroded hummocky terrain covered by a thin layer of organic material, subject to substantial reshaping by aeolian, fluvial, lacustrine, and karstic forces [38].

1.3.2 Dunes

Over 16,000 dunes have been imaged on Titan's surface [41], most of them classified as linear dunes akin to those found in Africa and Arabia. Linear dunes are the familiar dunes found in terrestrial deserts, long and narrow with ridges that align roughly in parallel as the result of winds blowing from two directions [30, 41]. Other types of dunes include reticulated dunes and featureless dune sands. Reticulated dunes are small areas of linear dunes exhibiting an orientation perpendicular to that of surrounding dunes, while dune sands contain broad lanes that can only be recognized in certain areas [30]. Though some isolated examples of higher latitude duneforms have been identified [42], dunes are rarely found outside of an equatorial band spanning from -30 to +30 degrees latitude. The general dearth of high-latitude dunes is attributable to a number of possible explanations: wind speeds may not be great enough to generate saltation, the dune-forming process of aeolian transport of loose materials; sand-sized particles may not exist with the same abundance as they do around the equator; these particles may be stablilized against movement by

moisture or topography; or polar hydrological processes may disrupt the long-term collection of such particles [42]. Alongside lakes, dunes are among the youngest of Titan's geological units. They also tend to overlay other features, including plains and hummock, and may feature actively shifting sands [42, 43].

Dunes' dark appearance in Cassini-Huygens imaging is consistent with a composition of organics precipitated to the surface after upper atmosphere photolysis [7, 30]. Estimates show that dunes cover 1.5 times as much surface area as the Sahara Desert and serve as a major surface reservoir of organics [7, 44]. Slopes of around 10 degrees and dune heights of 100 to 150 m place Titan's dunes on the same scales as those found in the Namib desert [45]. The global mean of dune spacing is around 2 km [45].

Dune orientation and interaction with topographical obstacles can provide constraints on local, regional and global wind patterns and directions [45]. Dunes appear to form and evolve due primarily to a dominant wind along the dune axis, combined with less influential seasonal or obtuse off-axis minor winds [45]. Global winds may generate net transport of particulates from higher latitudes to more arid equatorial regions. Dune sands seem to generally be transported from west to east [7], curving around western boundaries of obstacles and maintaining their orientation in the same way river water flows around islands or other obstructions [45]. This contradicts an expectation that surface winds at the low latitudes blow from east to west — potential explanations claim that the observed orientation and structure mirror occasional strong eastward gusts driven by atmospheric mixing [7, 46] or methane rainstorms [7, 47]. Given the global uniformity of dunes regardless of particulate supply or topographic obstruction, surface winds appear to maintain consistent strength, direction, and continuity [45].

Xanadu

Amid the dark band of equatorial dunes lies an anomalous, continent-sized bright region known as Xanadu. Its high backscatter is likely due to distinct chemical or physical composition from other regions or units on Titan, but it remains an area of mystery that defies expectations within the general framework of Titan knowledge [48].

At a size of 4,000 by 2,500 km, Xanadu has been informally divided into four subprovinces, each with its own defining characteristics. Xanadu features Titan's longest and best-developed fluvial networks, as well as its highest mountains and widest valleys, a confusion of planetary extremes that only serves to further pique interest in the region [48]. It also boasts Titan's highest concentration of impact craters — six of the nine confirmed impact craters and 49 unconfirmed candidates present globally [48]. Their conspicuous presence on Xanadu may indicate that the region is older than the rest of Titan [48, 49, 50].

Xanadu sits at a lower elevation relative to its surroundings, and it seems likely that the region's high backscatter and high-relief, mountainous terrain are products of a fundamentally different composition, perhaps tied to the region's geological and elevational positioning [48]. Modeling efforts have revealed a surface dielectric constant consistent with that of a water ice-based material mixed with or coated by a thin layer of organics [51], pointing to a potential composition of a fractured layer of water ice.

Why such a spatially large geophysical outlier lies within the dark, homogeneous band of organic equatorial dunes remains a topic of ongoing investigation. Xanadu's existence and nature may be tied to a combination of erosion and tectonics; *Radebaugh et al., 2011b* propose a process of subsurface contraction and expansion, followed by erosion and downward regional plate movement as a potential explanation for Xanadu's low elevation [48]. Under this theory, Xanadu is an old, eroded terrain continually being modified by fluvial and subsurface processes. Other explanations propose that Xanadu acts as a 'source' of materials, with winds generating a net flow away from the region that results in its thin organic blanket layer [48]. Some controversy exists over whether a 'methane drizzle'

falls specifically over Xanadu; if true, such a finding may indicate that the region perturbs meteorological systems, opening new avenues by which to explain its unique character [48].

1.3.3 Hummocky Terrain

Titan's hummocky terrain includes mountain chains and isolated peaks found at mid and high latitudes [30], as well as hills and mounds lacking the definition of mountains. Most of this terrain exhibits bright backscatter due to a composition of the fractured water ice that makes up Titan's lithosphere, or outermost crustal shell. Mountains that form via tectonic contraction can be characterized as exposed remnants of ancient bedrock [38, 49], and mounds and other hummocky features as eroded mountainous terrain perhaps covered by a layer of organic plains material [38]. The largest areal extent of the hummock is found within Xanadu [30].

Globally, the nature of Titan's elevated topography is relatively constrained: mountains reach only a few hundred meters in height and chains only a few tens of kilometers in length [7]. As on Earth, subsurface contraction and surface erosional processes are locked in an ongoing equilibrium that shapes Titan's mountains and other surface features, though erosion appears to be slower on Titan than on Earth due to the infrequency of precipitation [52]. Even at relatively slow rates, however, erosion appears to limit the vertical extent achievable by mountain peaks and ranges. Though water ice at Titan's low surface temperature is mechanically capable of supporting substantial elevated topography [52], erosional processes are apparently rapid enough to preclude the formation of anything more than sparse peaks across a generally flat surface. Estimates have placed the age of Titan's mountains within a planetologically young range of 20 to 100 million years, providing further evidence that the surface of Titan is less than a billion years old [52].

Cryovolcanism

Cryovolcanism — volcanic activity that produces some combination of water, ammonia and methane in gaseous or liquid form, rather than molten rock [53] — is common to satellites of the outer solar system, moons like Europa, Enceladus, and Triton. Defined more formally by *Kargel, 1995* as "the eruption of aqueous or nonpolar molecular solutions or partly crystallized slurries derived from partial melting of ice-bearing materials" [54], cryovolcanism generates plumes of liquid-vapor intermixed with solid fragments. It has long been suspected to play a role in resurfacing and methane replenishment processes on Titan [1]. Though the true role and location of cryovolcanic activity remains an unresolved question, favorable conditions supporting its potential occurrence include the presence of a global layer of liquid within Titan's interior [55].

The general trend, however, has been that as more data on cryovolcanism are uncovered and examined, potential cryovolcanic candidates seem less likely to, in fact, *be* cryovolcanoes [1]. The most likely sites of cryovolcanic activity exhibit characteristics similar to maar craters on Earth, including elevated rims, steep sides, and flat floors [7]. But criticisms of prior work examining these locations claim that observed morphologies attributed to the flow of ejected cryovolcanic material could have been produced by fluvial activity [7]. While cryovolcanic activity may have happened on Titan, it appears that it no longer is, and that fluvial, aeolian, and particle deposition processes dominate over endogenic events as the major means of resurfacing [53]. As *Lopes et al., 2013* put it, there is no "smoking gun" of thermal markers, signature plumes, or surface flow indicating active cryovolcanism [53]. But the question of cryovolcanism and its influence on the past remain important in ongoing efforts to establish a complete framework of Titan's climatic development and the nature of the relationship between its subsurface and atmosphere.

1.3.4 Labyrinth

Titan's so-called labyrinth terrain is characterized as locally elevated plateaux dissected by valleys carved by past fluvial activity [38]. Covering around 1.5% of Titan's surface, labyrinth is absent in the equatorial region and most prevalent in clusters at the mid and high latitudes, particularly at the south pole. Twice as much of the terrain exists in the southern hemisphere as in the northern, and it comprises about a third of all surface area between 80 and 90 degrees south [31]. At these latitudes, there exist a number of empty and filled lake basins surrounded by labyrinth, suggesting that labyrinth dissection by fluvial processes occurred prior to lake infilling, perhaps enabling it [31].

Three distinct types of labyrinth are present at various regions of the globe. Valleyed labyrinth is by far the most common type, comprising 68% of all labyrinth and defined by characteristic ridges and valleys arranged in rectilinear or radial structure [31]. Polygonal labyrinth — closed valleys with uniform spacing and orthogonal orientation relative to one another — appears mostly at high latitudes and makes up 18% of labyrinth. Finely dissected labyrinth is distinguished by a dense distribution of depressions which renders its features unresolvable by Cassini-Huygens or ground-based imaging technology [31]. An anomalous labyrinth region, Kronin Labyrinthus, has also been observed in the Xanadu province; encompassing just 3% of all labyrinth, it is notable for its non-uniform orientation and location at a low latitude [31]. Over 80% of intervalley spacings are less than 5 km, and individual labyrinth units feature consistent alignment patterns and spacing [31].

While the formation process of labyrinth is unknown, plains material is found within and at the termini of almost all valleys [31]. Labyrinth is one of Titan's oldest geological units [30], and its common makeup to that of plains implies that organic material appeared earlier in Titan's past than previously thought [31].

1.3.5 Craters

Though there are just 49 confirmed impact crater candidates scattered across Titan's surface [56], their structure and distribution nonetheless contribute to the moon's climatic story. All craters are less than 5 km in diameter, indicating that larger bolides tend to combust or break down in Titan's thick atmosphere before they reach the surface [57].

We should, however, expect Titan to be as populated with craters over a given area as nearby pockmarked moons, such as Rhea and Tethys. Titan's paucity of observed craters relative to other satellites in the Saturnian system suggests that its surface has been substantially reworked by erosive processes, and that craters are likely to be submersed by dunes and lakes [56].

Most of Titan's craters are found on the leading hemisphere in a relatively well-defined range across the low and mid northern latitudes. Few have been observed south of -30 degrees, and the dearth of craters at northern polar latitudes is perhaps attributable to infilling and submergence by hydrocarbon liquid lakes [56]. While the dunes are essentially not cratered, the Xanadu province is home to a conspicuously high proportion of global craters, strengthening theories that it is geologically older than other regions and has undergone less refacing.

The rims of most craters are composed of crustal water ice and organics [38, 58]. The effects of fluvial transport and mass wasting processes — downward flow of material due to the influence of gravity — are evident in the structural decomposition of many rims. Crater fill material is deposited by fluvial, aeolian, erosive and depositional processes on long timescales so that this material increasingly resembles the surrounding terrain [58]. Only some craters feature ejecta blankets from the impacts themselves [58], but it is likely that such blankets have been overlain with other material by forces similar to those that reshape crater interiors. Spectral examination reveals that 'chemical weathering' occurs in

the equatorial regions. Despite only sporadic precipitation, the mixture of water ice and organics exposed by the initial impact has its organic components gradually reduced by methane rainfall, leaving water ice as the primary observed constituent [58].

1.3.6 Lakes and Seas

As the only stable bodies of surface liquid in the solar system outside of Earth, Titan's lakes and seas are tantalizing objects capable of inspiring both crucial scientific study and unadulterated wonder. Composed of a ternary mix of methane, ethane and nitrogen [59], lakes and seas cover just over 1% of the surface and are restricted to latitudes poleward of 55 degrees [59]. The polar regions contain over 650 dry or filled basins, though there is a substantial north-south disparity: 97% of all liquid by area is sequestered in the north, while only nine filled lakes reside in the south [30]. Surface liquid covers just 0.25% of surface area poleward of 55 degrees in the south, but 11% in the north [40, 59, 60]. The asymmetric distribution of this liquid at the poles is a major focus of this work, to be expanded upon in section 1.4 and chapters 2 and 3.

The three largest northern seas — Kraken, Ligeia, and Punga Maria — account for over 80% of all liquid [30], but the southern pole is home to only one large body, Ontario Lacus, as well as a number of observed empty basins posited to be paleoseas filled at some point in Titan's past [35, 61]. Two empty basin regions within the equatorial band, Hotei Regio and Tui Regio, are surrounded by converging fluvial networks resembling those found near filled high-latitude lakes. These basins have been interpreted as possible low-latitude paleoseas [62].

The total volume of the lakes and seas has been estimated at 70,000 km^3, just 15% of the volume of atmospheric methane, suggesting that surface liquids are not influential in global climate processes and precluding their involvement as replenishing sources of atmospheric methane [59]. Areal footprints of these bodies range from a few square kilometers to over 500,000 km^2 [59], around five times the size of Lake Superior. Bathymetric measurements of the three largest seas were taken by Cassini-Huygens, revealing a depth of around 300 m at Kraken Mare [59].

The methane-based lakes and seas constitute an essential component of wider ongoing study of the nature, transport, and replenishment of Titan's global methane hydrological cycle. In and of themselves, however, these bodies also hold mysteries of their own concerning structure, composition, and interconnectedness that have yet to be resolved. Perhaps the most pressing outstanding question is that of Titan's 'missing ethane'. Ethane, the main byproduct of methane photolysis, was spectrally detected by Cassini-Huygens as a constituent of Ontario Lacus [63] after *Lunine, Stevenson & Yung, 1983* [64] predicted, based on the amount of ethane generated by atmospheric chemistry, that a global ocean several meters deep would cover Titan's surface. No such ocean exists; in fact, the disparity between observed and model-predicted atmospheric ethane is on the order of 10^4 [63]. This would appear to suggest that most ethane resides in liquid form at the surface, but the volume of ethane contained within lakes, seas, and craters constitutes only 8.2% of possible global production, an unfeasibly low number [63]. Given that it is not distributed throughout the atmosphere or on the surface, *Gilliam & Lerman, 2016* showed that the entire global ethane budget could, theoretically, be accommodated by the porous, icy layer of the top 2 km of Titan's crust [63]. The unexplored subsurface is likely to serve as a storage reservoir, trapping ethane in molecular bindings known as *clathrates* and providing a potential explanation for the riddle of Titan's ethane.

A number of researchers, most notably *Hayes et al., 2017*, have examined the subsurface relationship between lacustrine systems, determining that northern seas are consistent with an equipotential surface, meaning they lie at the same elevation [65]. Empty lake floors of sharp-edged depressions (SEDs) are generally higher than the liquid elevation

levels of nearby lakes and seas, implying a subsurface connection between them. Even more promising, a number of filled lakes have been found to lie hundreds of meters above this sea level, indicating that they may be part of a separate system of basins connected endogenously [65]. Though the formation processes and materials of these systems are still unknown, the possibility of their subsurface linkages could provide more insight into the nature of Titan's interconnectedness, from interior to surface to atmosphere.

1.4 Methane Cycle

Along with its stable surface liquids and robust atmosphere, Titan is frequently labeled the most Earth-like body in the solar system for its active methane-based hydrological cycle. In a role similar to that of Earth's water cycle, this global system drives processes of precipitation and evaporation, governing the spatial distribution of surface liquids at various latitudes. It ties the atmosphere, surface and subsurface together, guided by an array of short- and long-term climatic processes and Titan's orbital configuration, and it is largely responsible not only for Titan's unique topography and surface features, but also for shaping the past and future evolution of energy and moisture transport.

Parallels between the only stable moist weather systems in the solar system can be easily drawn. Conditions on Titan hover near the triple point for methane, the temperature and pressure at which solid, liquid and gaseous forms of methane can coexist, allowing all phases to impact the climate similar to the way all phases of water contribute to climatic processes on Earth [66]. Methane also contributes to the very structure of the atmosphere: without its presence, the atmosphere would be dramatically thinned and would cool so sharply that nitrogen would freeze onto the surface in a phenomenon similar to that found on Neptune's moon Triton [67]. Almost all Titan's observable methane is held within the atmosphere — roughly seven times as much as is found on the surface [66]. Were it all to suddenly condense into liquid, atmospheric methane would form a global ocean layer four to five meters deep across the entirety of Titan's surface [66, 68]. Like water on Earth, Titan's methane serves as both a significant contributor to the global greenhouse effect and the primary condensible substance that precipitates onto the surface [66].

Though methane's distribution across the surface and atmosphere is well-understood, identifying the source of its continued replenishment remains perhaps the greatest unresolved question facing Titan scholars. Without replenishment, photolysis would destroy Titan's global budget within just tens of million years [66]. Stable surface bodies, at about 15% the methane content of the atmosphere, lack the volume to provide continued replenishment to the degree observed [69], and a dearth of observed impact craters indicates that comets and asteroids do not penetrate Titan's atmosphere frequently enough to serve as long-term sources of methane [66]. The most widely supported theory of methane replenishment involves outgassing from Titan's interior, where both methane and ethane are posited to be locked away within a reservoir of clathrates [59, 70, 71] or within a water ocean [72, 73] kilometers below the surface. This subsurface methane could be drawn upward by a chemical reactive process known as serpentinization and expelled by cryovolcanism [66, 70]. No firm evidence for surface cryovolcanic activity has been identified [53], but Cassini-Huygens detected ^{40}Ar, a decay product of ^{40}K, providing some evidence of interior outgassing [9].

Cassini-Huygens also provided evidence of the hydrological cycle's activity, revealing surface darkening and fading consistent with methane rainstorms. It observed a number of well-known fluvial effects, including deltas [74], alluvial fans [39, 75], and reworked floodplains [76]. Fluvial features, including networks of channels that stretch hundreds of kilometers [77], are found at all latitudes [78]. At the northern pole, some of these channels are confined within steep-sided canyons 300 m deep [79]. Rainstorms tend to

occur in localized bursts of infrequent but powerful downpours [80]; raindrops are so slow to reach the ground from the mid and upper atmosphere that storms often gather and dissipate before precipitation falls to the surface [59]. Several convective events occur every Earth year at a given location [59], typically at tropical and polar latitudes [81]. It is estimated that between 40 and 400 hours of rainfall at all latitudes [82] drop an average of 18 cm of rain per Titan year [80]. Just 0.7% of the surface is wetted over the course of six Earth years, meaning it takes roughly 1,000 years to wet the entire surface [83]. During summertime at the high latitudes, poles receive enough rain to outweigh evaporation and infill lake basins, even as low latitudes dry quickly [84]. This may lead to compositional disparities where lakes and seas closer to the poles contain higher methane content [82]. Subsurface liquid may have compositional effects at all latitudes, particularly the poles, where local connectivity of basins may indicate the presence of a methane table [9, 60, 85].

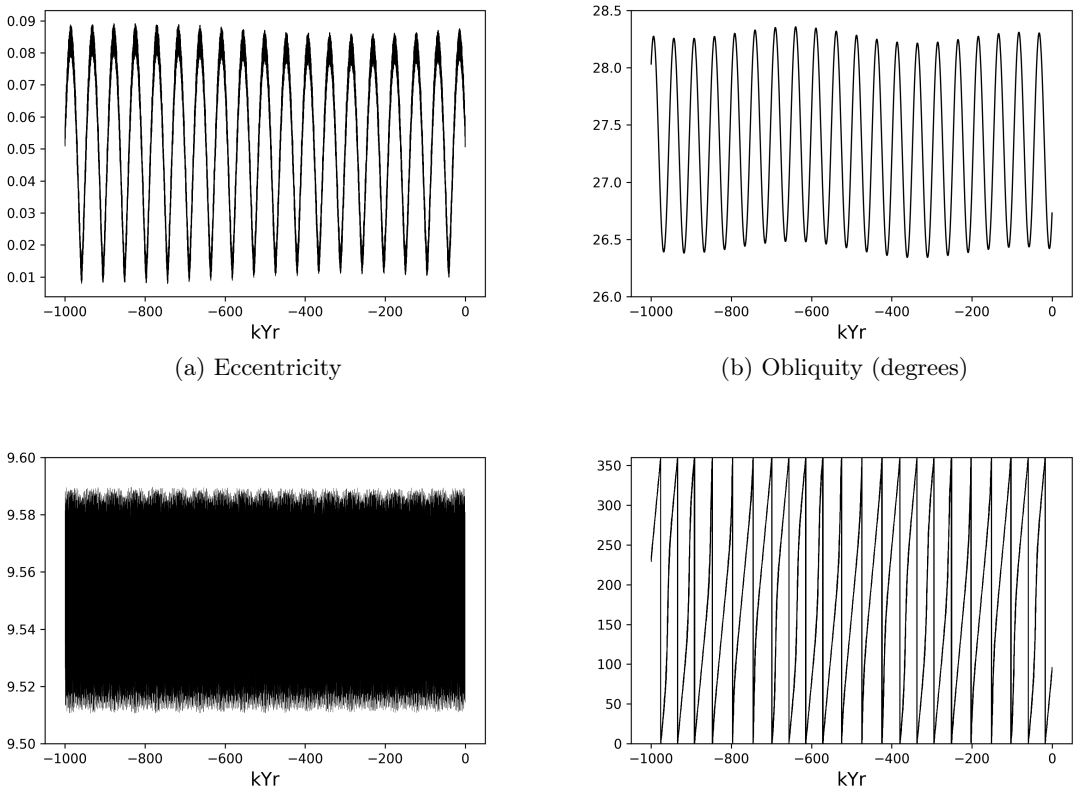

(a) Eccentricity

(b) Obliquity (degrees)

(c) Semi-major axis (AU)

(d) Solar longitude of perihelion (degrees)

Figure 1.3: Orbital characteristics of Titan over the past million years. The variance observed in these parameters drives Milankovitch-like cycles, which contribute to asymmetric polar moisture transport and pole-to-pole methane distribution.

While precipitation events develop on hourly timescales, global moisture and energy distribution is governed by seasonal effects across tens of years and orbital effects across tens of thousands. Cloud cover shades less than 1% of Titan's surface [86], and clouds' locations point to seasonality as an important driver of weather [66, 87]. Lower latitudes consistently receive more insolation than do higher latitudes, generating net heating over the equator that, in the absence of atmospheric mixing, would result in a difference in surface temperature of around 20 K between the poles and equator [84, 88]. The true observed difference, however, is just 2–4 K, signaling that compensatory transport of heat to the poles homogenizes surface temperatures [84]. In a Titan year, net methane transport

is estimated to be on the order of 5×10^{14} kg from the north pole to the south [89]; over many years this accumulation may gradually fill previously empty basins [35].

But the distribution is not perfectly symmetric. Southern summers are shorter and more intense, receiving an additional 1.5 Wm^{-2} of incoming solar flux, a difference of 24% [33]. *Aharonson et al., 2009* propose that insolation-driven processes of evaporation and precipitation account for an asymmetric accumulation of methane and severe disproportion of surface liquid found at the northern pole. The hemisphere to which methane mostly migrates oscillates based on the north-south imbalance in peak summer insolation [34]. Saturn's rate of perihelion precession — as it orbits, the rate at which the line connecting its closest and furthest points from the Sun gradually rotates — induces a cyclic shift of the observed asymmetry from pole to pole at a period of 45,000 years [33]. These cycles dictating long-term fluctuation of moisture imbalance between poles are governed by eccentricity, spin axis, and other orbital variations, and are analogous to Croll-Milankovitch cycles on Earth, which contribute to reversals in the magnitude and direction of seasonal effects over kiloyear climatic processes [34, 33, 89, 90, 91]. These cycles may explain the presence of empty paleosea basins at the southern pole, which simulations show to have been filled in Titan's past when methane was congregated in the south [34].

Titan's stratospheric superrotation, an atmospheric property whereby the average angular momentum of a body's atmosphere exceeds that of the body itself at the equator, points to the influence of nonaxisymmetric atmospheric disturbances, otherwise known as atmospheric eddies [89]. *Lora and Mitchell, 2015* illuminate the mechanism behind Titan's unequal methane distribution using a three-dimensional general circulation model (GCM) that incorporates eddies to demonstrate that their presence induces hemispheric asymmetries in methane distribution as moisture is transferred from the poles to the mid latitudes [91]. Eddies are more intense in the south than the north, leading to the observed net northward transport.

Chapter 2

Theory

Having reviewed Titan's historical, morphological, and climatic background, we turn now to the motivation and theory behind this project. Prior investigation has produced a granular picture of Titan's dynamics and surface-atmosphere interaction through models of global circulation, which simulate how solar and orbital forcing drive the dispersion of energy and moisture. The most useful of these models are three-dimensional, incorporating not just latitudinal but altitudinal and longitudinal dependence across the surface and atmosphere. These more complex models balance the influence of radiative transfer — incoming and outgoing radiation — with that of winds, temperature gradients, surface topography, subsurface effects, moisture, and chemical and physical processes. They are the most essential tools for researchers to study Titan's evolution and tinker with its parameters in order to deeply explore and understand its properties as a system.

These models come with severe computational costs, however, often requiring so much time and processing power to run that those using them can only examine snapshots of Titan's past or glimpses, under a set of predefined circumstances, of its future.

In this work, we construct an energy balance model (EBM) — a smaller scale, one-dimensional version of a global climate model — in an effort to strike a balance between functionality and explanatory power. By exploring via rapid and inexpensive computational processes the nature of key meteorological parameters as they vary under an assortment of Titanian conditions, we put forth a viable model for understanding the latitudinal profiles of energy, temperature, and moisture in a straightforward, flexible manner. The model is built to corroborate meteorological simulation results from Earth, prior to being applied and calibrated to Titan. Ultimately, we utilize it to thoroughly explore the sensitivity of unknown Titan parameters, including the diffusion coefficient, gross moist stability, and relative humidity profile, examining how energy and moisture distribution respond to variations in these parameters. The following chapter provides a brief overview of the motivation to create such a model and the theoretical pillars of meteorology and planetary physics upholding its implementation.

2.1 Motivation

General circulation is defined as the time-averaged motion representing the long-term statistical behavior of a planetary atmosphere [92]. General circulation models (GCMs) numerically integrate equations of fluid flow in order to simulate the evolution and variation of the general circulation. The solutions to these models tend not to be overly sensitive to initial conditions [92].

GCMs use various types and resolutions of coordinate grids to define position by longitude and latitude. The model is calibrated with data on surface pressure, winds, temperature, and humidity at gridpoints representing a collection of locations [93]. The for-

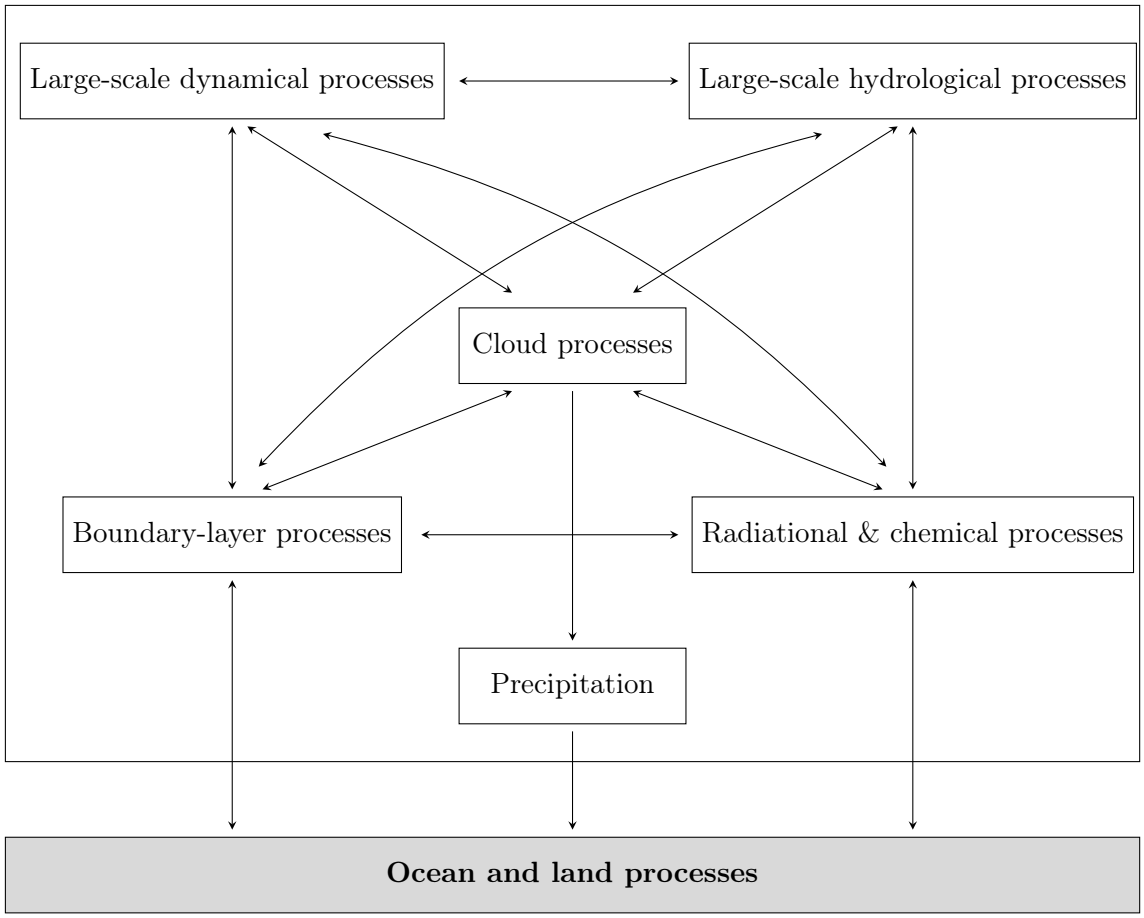

Figure 2.1: The interactions of basic processes in the climate system. Sourced from *Mechoso et al., 2015* [92].

mulation of how these variables are parameterized is crucial to model quality, separating high-resolution models from those that are less informative. The various physical processes and their interplay has been mapped in the simple diagram shown in Figure 2.1.

The first successful results from a GCM-type model came in the 1950s, when a simple dynamical model was able to predict 24-hour forecasts monitoring daily weather changes. Later, these same early iterations were able to explain observed features of general circulation whose causes had previously been subject to mere speculation [92]. Even as model complexity and supercomputer performance have surged over the course of decades, short-term weather and climate predictions remain a primary application of GCMs.

The other notable application, which the model in this project exemplifies, is long-term climate system development and variability. Results are typically achieved by allowing a GCM simulation to run until it has achieved quasistatic equilibrium [92]. This state is then defined as the planet's climate; from there, individual parameters can be altered in order to explore their effects on the climate in comparison to the baseline. This method of investigation has been used to examine the atmospheric and climatic impacts of the La Niña and El Niño phenomena in the Pacific Ocean, as well as a number of other ocean processes [92].

The wealth of data provided by Cassini-Huygens allows researchers to sketch a useful profile of Titan's climate, but GCMs permit the nuanced analysis of the mechanisms behind climatic processes that is necessary to fully explain the moon's unanswered questions. After *Aharonson et al., 2009* [33] posited that asymmetric distribution of polar moisture may result from orbital processes that reverse themselves with a period of 45,000 years,

a number of subsequent investigations utilizing GCMs followed. *Schneider et al., 2012* [90] demonstrated that moisture accumulates preferentially at the northern pole as it is drawn away from the southern pole by Saturn's current orbital configuration. *Lora et al., 2014* [34] confirmed that this trend oscillates between the two poles on kiloyear timescales in a pattern similar to Croll-Milankovitch cycles on Earth. Most recently, *Tokano 2019* employed a GCM to examine the role that hemispheric asymmetry in surface topography might play in governing moisture transport and distribution, a basis of investigation that underscores the ability of GCMs to incorporate the effects and variations of all aspects of climate.

While these insights supported Aharonson's claim, simulations also undercut the argument: *Schneider et al., 2012* [90] found that orbital dynamics would give rise to a hemispheric imbalance in precipitation but not evaporation, meaning other processes, perhaps seasonal, must also be present to account for the observed asymmetry. *Moore et al., 2014* [76] expressed doubt over the unilateral influence of Croll-Milankovitch-like cycles, given that certain lacustrine properties point to their evolution over timescales greater than 45,000 years [94].

As a one-dimensional EBM rather than a three-dimensional GCM, the model realized in this project cannot replicate the complexity of the results that constitute well-founded, well-analyzed theories of hemispheric asymmetry due to orbital configurations. As established by *Lora and Mitchell, 2015* [91] only GCMs can incorporate the three-dimensionality of atmospheric eddies, small-scale disturbances in air and fluid currents that vary from the general flow trend. The precise purpose of EBMs is to capture net trends, averaging over the asymmetries that emerge from disparities in eddy effects in an effort to illuminate general patterns. At vastly lower computational costs, models like ours can be flexibly adjusted in order to rapidly investigate the sensitivity of a climate system to a range of parameter changes. This includes the illumination of kiloyears-long trends at smaller time steps and the straightforward implementation of extreme cases, such as an aqueous world.

2.2 Meteorological and Physical Background

Insolation and Energy

The primary source of energy driving atmospheric processes is insolation. Incoming solar radiation of all electromagnetic wavelengths hits the top of the atmosphere; some of it is reflected and scattered, while some of it penetrates fully to warm the surface and is absorbed by the planetary system.

No body is heated equally, however. The three factors responsible for variations in the amount of sunlight include angle of insolation, time of day, and latitude. Angle is a manifestation of seasonal effects — summer days on Earth, for example, are longer and brighter because axial tilt results in the Sun shining more directly on the summer hemisphere for a greater duration. The angle of insolation is diminished from its summer solstice peak during equinox and winter solstice.

Saturn features an axial tilt of 26 degrees — as compared to Earth's tilt of roughly 23.5 degrees — that drives seasonal insolation effects on Titan. These effects are exacerbated and manifested on longer timescales by Saturn's distance from the Sun and Titan's orbit around it: a Titan day is equivalent to 15.95 Earth days, while a Titan year lasts 29 Earth years.

Latitudinal variation governs insolation on both moons and planets, and it is crucial to the model in this project. A body's spherical geometry means that it only intercepts a portion of all solar irradiance, which strikes equatorial latitudes more directly. At higher latitudes, the same amount of sunlight is diffused across a greater cross-section of surface area, resulting in less intense heating.

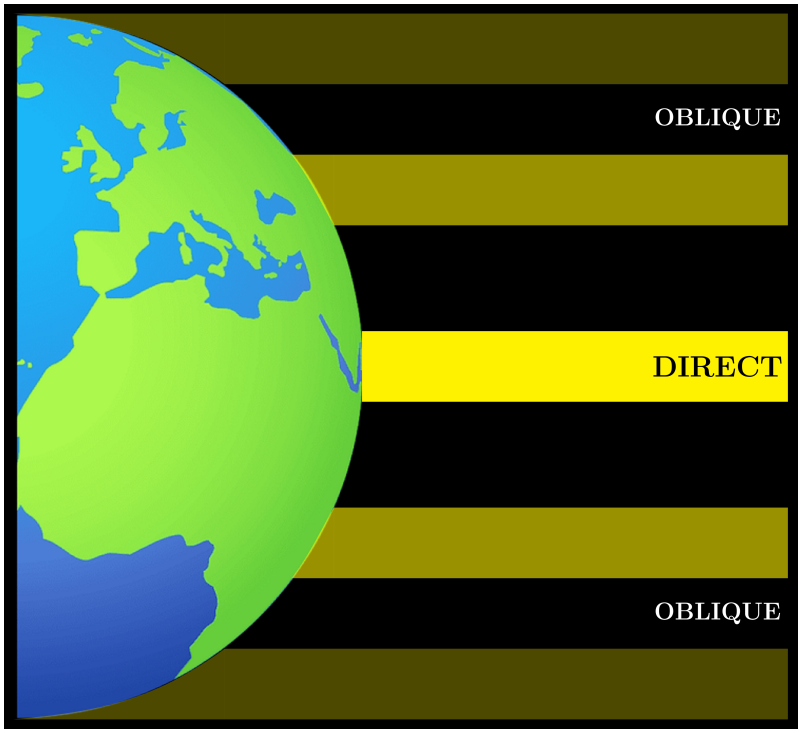

Figure 2.2: Insolation strikes the Earth's surface at different angles depending on latitude. Solar energy is more concentrated near the equator, where it irradiates the surface perpendicularly. At the mid latitudes and poles, however, the same cross-sectional profile of sunlight is diffused across a greater areal extent due to the angle at which it strikes, leading to less concentration and warming.

Since a body is not heated equally across latitudes, planetary systems constantly redistribute energy from the warmer low latitudes to the colder poles, and from the surface and atmosphere back out to space. The metric measuring the proportion of incoming energy that is radiated back into space, known as *albedo*, is an important feature on any body. Albedo values vary across material types — ice, for example, has a higher albedo than water or land cover. In higher resolution EBMs for Earth, albedo values of different surface materials and the transition areas between them are carefully defined to generate as true a replication of reflectivity as possible. The globally-averaged value of albedo on Earth is 0.3; averaging is used in our model for Titan as well, since its surface features are less well-mapped and distinct than those found on Earth. The working value for Titan's global albedo sits at 0.22.

The constant inflow and outflow of energy from the system is known as its *energy budget*. When insolation and outgoing radiation at the top of the atmosphere are balanced, a body achieves a stable temperature in a state of *radiative equilibrium*. If the source of either incoming or outgoing radiation is disrupted or altered, the climatic processes governing energy distribution compensate in order to re-settle into radiative equilibrium, without which a body's temperature would rise unimpeded. The equilibrium temperature is the atmospheric temperature at which this balance is achieved — for Earth, a value of 255 K. Molecules like carbon dioxide, water vapor, and methane absorb thermal energy radiating from the surface into space, trapping that energy in the lower atmosphere and radiating it back out in all directions. This produces the greenhouse effect, which raises Earth's average surface temperature to around 288 K. Owing to an atmosphere that blocks around 90% of what faint solar energy it receives, Titan's average surface temperature is a frigid 92 K.

We denote the total amount of solar energy received at the top of a body's atmosphere per unit time per unit area as the *solar constant*. This value has been measured for Earth by satellite as 1362 Wm^{-2}, though it dips to 1361 Wm^{-2} when Earth is at its maximum distance from the Sun. This value, however, is measured on a theoretically flat surface perpendicular to the incoming radiation. We know, based on the curvature of the spherical Earth, that this idealized circumstance applies only for a narrow sliver of all latitudes. For the majority of latitudes, insolation strikes at an angle.

A more apt metric of incoming insolation is the non-idealized global average of how much solar energy actually strikes the upper atmosphere. At any given time, solar flux only irradiates a circular cross-section of the Earth, not the entire sphere. The portion of the planet actually receiving insolation is a circle with area πR_e^2, where R_e is 6.37×10^6 m, the radius of Earth. The total surface area of Earth is given by $4\pi R_e^2$. The proportion of total surface area for which the circular cross-section accounts is the same proportion of the solar constant that actually strikes Earth, averaged globally. We find that

$$\frac{\pi R_e^2}{4\pi R_e^2} = \frac{1}{4},$$

meaning Q_0, the average solar irradiance, is given by $\frac{1362}{4}$ Wm^{-2}, or 340.5 Wm^{-2}.

These values can be calculated for Titan based on the moon's distance and radius. We first recalculate the total incoming solar energy. Earth is 1 AU away from the Sun, while Titan is, on average, 9.58 AU away. Insolation is proportional to the inverse square of distance, $\frac{1}{d^2}$, so Titan should receive an amount of insolation equal to $\frac{1}{9.58^2}$ times that received by Earth. We find the value to be

$$\frac{1}{9.58^2} \cdot 1362 = 14.84.$$

Rounding to account for the non-constant distance from the Sun of Saturn's elliptical orbit, this value becomes 15 Wm^{-2}. Using the same reasoning as before, we divide by four to obtain Titan's average global insolation, 3.75 Wm^{-2}.

Hadley Cell

Uneven heating from insolation drives various processes of atmospheric circulation as the climate system redistributes heat from warmer to cooler latitudes. Three major 'cells' on Earth divide the troposphere into regions of winds. The largest and most important of these is the Hadley cell, which acts at the low latitudes to draw energy from the equator poleward. In doing so, the Hadley cell engenders an array of weather patterns as well as the 'trade winds', a band of winds that blow from the high pressure subtropics to the low pressure zone at the equator, guiding centuries of seafaring voyages.

Figure 2.3 shows a simple diagram of circulation as governed by the Hadley cell, which extends from the equator into the subtropics, roughly 30 degrees latitude in both the northern and southern hemisphere. Since the highest concentration of insolation occurs at low latitudes, air at the equatorial band — known as the intertropical convergence zone (ITCZ) — is directly heated, causing it to rise into the troposphere. At this altitude it is pushed toward higher latitudes by the continued heating and rising of equatorial air below it. As it travels, radiation cools the air, causing it to sink. The air's contraction as it sinks from high altitudes corresponds to an increase in its temperature and induces a decrease in its relative humidity, the proportion of moisture the air contains. Pressure at the air's descending latitude in the subtropics is high while pressure at the equator is low; the tendency to flow down that pressure gradient pulls the air back toward the equator, and moisture evaporates into it as it goes. The convergence of moist air at the equator results in heavy precipitation, giving rise to the ITCZ's humid conditions as the wettest

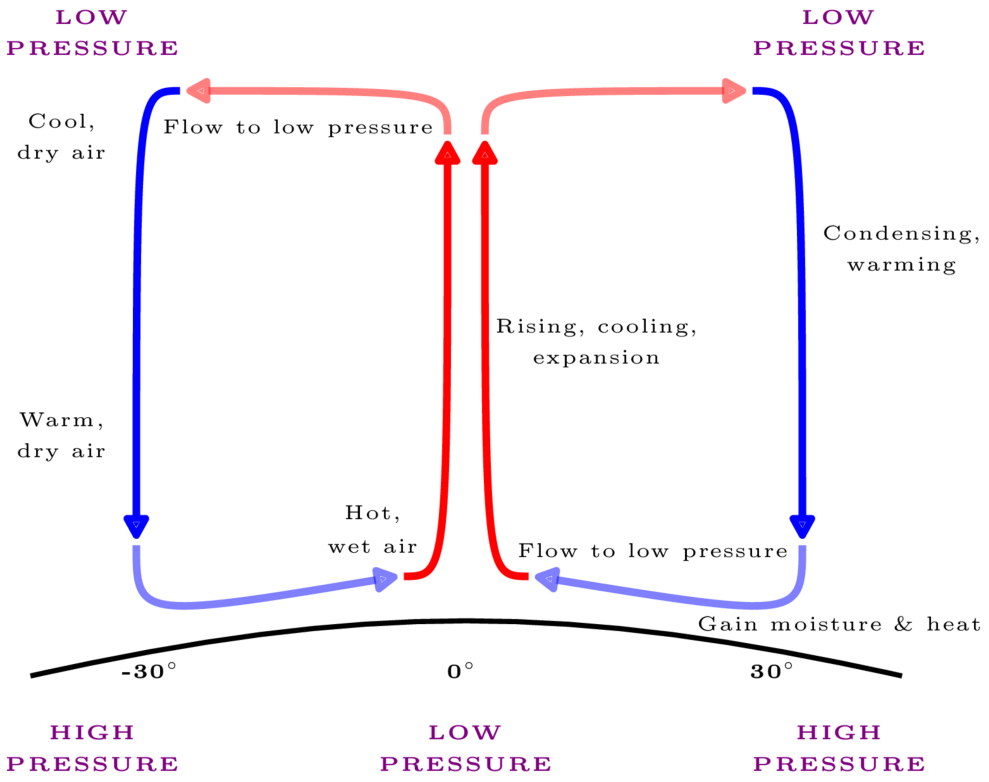

Figure 2.3: Earth's Hadley cell draws warm, dry air along the surface from the high pressure subtropics to the low pressure equator, where it dumps precipitation within the ITCZ before rising, expanding, and being pushed back to the subtropics at high altitudes.

latitudinal band on Earth. This process takes place in both the northern and southern hemispheres.

Though the two bodies are distinct in their atmospheric structures and processes of circulation, lessons from Earth-based dynamical theory could be applied to Titan. The polar confinement of surface liquids suggests that an analogue of a stronger, more latitudinally extended version of the Hadley cell could be responsible for concentrating moisture at these areas. The mechanisms governing such a process would, of course, be incongruent between the bodies — though equatorial latitudes are the wettest regions on Earth, they are the driest areas of Titan, subject to a global minimum in relative humidity and little more than scattered precipitation. Titan's slow rotation and the vertical scale height of its atmosphere — at least three times that of Earth's, if not greater [14] — induce a nearly-global Hadley cell analogue. In our model, the latitudinal Hadley cell extent σ is a free parameter whose sensitivity is explored.

Moisture and Humidity

Comprising a crucial component of this work are the energies and energy fluxes that both govern and measure the efficiency of global moisture distribution. Our model is predicated upon the numerical integration of a differential equation of moist static energy flux, and the final output features a recursive function that evaluates the sensitivity and physical constraints of Titan's global relative humidity profile. Both are intimately linked to the mechanisms behind processes of moisture distribution.

The mixing ratio for a parcel of air of a certain volume, denoted w, is defined as the ratio of the mass of water vapor to the mass of dry air.

$$w \equiv \frac{m_v}{m_d} \tag{2.1}$$

When neither condensation nor evaporation occur, this ratio is constant. The mass of water vapor within a unit mass of air — that is, dry air plus water vapor — is known as *specific humidity* and given by

$$q \equiv \frac{m_v}{m_v + m_d} = \frac{w}{1+w}. \tag{2.2}$$

In contrast to the true mixing ratio w, which measures the actual proportional mass of moist and dry air, the saturation mixing ratio w_s provides a baseline relative to an idealized parcel of air saturated with moisture. If the floor of an enclosed box is covered by a plane of water at temperature T, that water will begin evaporating. As more water molecules are released into the air, the total number of molecules in the box rises, raising the water vapor pressure e. Even as it evaporates, water will also be condensing back from vapor into liquid. When the rates of evaporation and condensation are equivalent, the air is *saturated* with respect to the plane of water at temperature T. The pressure exerted by the water vapor in the air is e_s, the *saturation vapor pressure*.

The saturation mixing ratio w_s is the mass of moist air that is saturated in this way, divided by the mass of the dry air

$$w_s \equiv \frac{m_{vs}}{m_d}. \tag{2.3}$$

Maintaining the same pressure and temperature, *relative humidity* is nothing more than the ratio of the mixing ratio w to the saturation mixing ratio w_s, equivalent to the ratio of vapor pressure e to saturation vapor pressure e_s.

$$RH = \frac{w}{w_s} \simeq \frac{e}{e_s} \tag{2.4}$$

In an intuitive sense, relative humidity represents the proportion of water vapor present in the air, relative to what that same parcel of air could hold at its given temperature. Given that it involves the masses of dry and saturated air, relative humidity is sensitive to atmospheric composition. On Earth, the globally-averaged relative humidity hovers around 0.8, with discrepancies depending on whether the value is measured over land, ice, or water. Titan's local, near-surface relative humidity was measured at around 0.5 by the Huygens probe at the mid latitudes, but this value has been shown to increase toward the poles as insolation diminishes and moisture is increasingly prevalent [95]. As shown by *Lora & Ádámkovics, 2017* and thoroughly explored later in this project, Titan's relative humidity profile is an inverse of that found on Earth, where the equatorial latitudes are far wetter than the poles.

Though it is no less essential to our model than relative humidity, *moist static energy* is a far more abstruse concept. Moist static energy and its constituent parallel, dry static energy, are thermodynamic properties of air, meaning they specify or describe the state of the system. A closely associated type of thermodynamic process is known as an *adiabatic process*, one in which a system does not exchange any heat or mass with its surrounding environment and any energy loss in the system's internal energy is equivalent to work done by the system on its surroundings.

Consider an idealized parcel of air, infinitesimal in its dimensions, that is thermally insulated from its surroundings and moving at a slow enough velocity that its macroscopic kinetic energy represents a negligible fraction of its total energy. Raising this parcel upward through Earth's atmosphere adiabatically would cause its volume to expand as pressure decreases, leading to a drop in temperature as constriction on air molecules is relaxed and

internal energy decreases. In expanding, the parcel conducts work on its surroundings, and the subsequent conserved quantity is known as moist static energy, given by

$$h = c_p T + gz + L_v q \tag{2.5}$$

where T is the temperature of the air parcel, g is acceleration due to gravity, z is altitude, and q is specific humidity. The specific heat capacity, c_p is defined as the amount of heat needed to produce a unit Kelvin change in the temperature of a substance. The latent heat of vaporization, L_v, is the amount of heat required to transform a given quantity of liquid into vapor. The first term on the righthand side of the equation, $c_p T$, is the internal energy of one unit mass of air. Together, the first two terms on the righthand side, $c_p T + gz$, constitute *dry static energy.* When a parcel of dry air is raised adiabatically through the atmosphere, potential energy increases with altitude. This change to the system is compensated by a decrease in internal energy as temperature falls; overall, the dry static energy is conserved.

When moisture is present in the parcel, energy is budgeted across all three righthand-side terms. The increase in potential energy is balanced by decreases in internal energy and latent heat content, and the sum of the terms is once more conserved, this time as moist static energy.

In our model, moist static energy is defined without its middle term due to the fact that the height of the atmosphere is not parameterized within a one-dimensional model. As such, there is no altitudinal dependence or influence of gravity; the quantity measured is near-surface moist static energy. While moist static energy plays a role in partitioning the mass transport circulation effects of the Hadley cell, it is moist energy flux that lies at the heart of the model.

Chapter 3

Model

To examine Titan's climate, we initialize a one-dimensional model of the latitudinal dependencies of energetic, thermal, and hydrological processes, allowing their sensitivities and interactions to be explored at low computational costs. The model is calibrated on known climatological results for energy distribution on Earth, then applied to conditions on Titan and tuned to understand the influence of moisture-related free parameters whose exact values are currently unknown. By numerically integrating differential equations that evaluate moist static energy flux and its relationship to solar heating, the Titan iteration accurately replicates known temperature, energy, and moisture profiles. Implementing a recursive function, we show that the model permits the natural emergence of a convergent solution for the relative humidity profile, matching that observed by data. The sensitivity of this profile is also analyzed, and physical processes behind its response explored, illuminating the intuition behind planetary constraints governing moisture distribution.

The model is developed in Python, with source code transferred from its initial form in R, where it was created by Tyler Kukla and Daniel Ibarra in 2018 and based on the insights of *Roe et al., 2015* [15], *Held, 2001* [96], and *Siler et al., 2018* [97]. Input characterizing the latitudinal dependence is the sine of latitude, represented as xin, a grid that ranges from -0.999 to 0.999 in increments of 0.001. This corresponds, approximately, to a 1000-node grid of latitudes spanning -90 to +90 degrees. In the sine form xin, endpoints have been eliminated to avoid singularities.

The central pillar of the model is the EBM function itself, which solves a boundary value problem — a system of ordinary differential equations featuring solution and derivative values at every point — in order to relate insolation and radiative equilibrium to surface temperature and moist static energy flux, the rate of poleward energy flow with respect to latitude. The complementary hydrological function builds off the EBM output by numerically integrating the moist static energy flux equation and calculating an array of other thermodynamic characteristics of the planetary body. These features include moist static energy and moist static energy divergence, as well as net surface moisture accumulation and latent heat flux, the energy flux transfer between surface and atmosphere associated with processes of evaporation and condensation.

3.1 EBM

The EBM function solves the boundary value problem with generalized inputs x, representing latitude, and y, whose subcomponents represent temperature and moist static energy flux. The net solar forcing term at the heart of the EBM function is the balance between incoming insolation and outgoing longwave radition, given by

$$I - M = Q_0 S(1 - \alpha) - (A_0 + B_0 T) \tag{3.1}$$

Constant	Description	Earth	Titan	Units
c_p	Heat capacity	1004	1000	J kg^{-1} K^{-1}
w	Mixing ratio	0.622	0.571	unitless
L_v	Latent heat of vaporization	2.45×10^5	5.5×10^4	J kg^{-1}
e_0	Saturation vapor pressure	611.2	10600	Pa
p_0	Surface pressure	1.013×10^4	1.5×10^4	Pa
g	Acceleration due to gravity	9.81	1.35	m s^{-2}
R_v	Gas constant of vapor	461.5	518.2	J kg^{-1}
R	Radius	6.37×10^5	2.57×10^5	m
ρ	Liquid density	1000	450	g m^{-3}
α	Albedo	0.3	0.22	unitless
Q_0	Global average insolation	340.5	3.75	W m^{-2}
m_0	Mean molecular mass	28	27.1	g mol^{-1}
Ω	Rotation rate	7.27×10^{-6}	4.56×10^{-7}	rad s^{-1}
T_0	Triple-point temperature	273.14	90.68	K

Parameter	Description	Earth	Titan	Units
Γ	Gross moist stability	1.5×10^3		J kg^{-1}
D	Diffusion coefficient	1.16×10^6		m^2 s^{-1}
RH	Relative humidity	0.8		unitless
σ	Hadley cell extent	0.3		unitless

Table 3.1: Parameters and constants for Earth and Titan, with units and descriptions. Parameters whose values for Titan were later expressed and tuned by model outputs are left blank.

where the energy source term I is the product of the global average insolation constant Q_0 and the percentage of energy not reflected back into space $1 - \alpha$, multiplied by S, the Legendre polynomial best approximating insolation received by a spherical body. As originally derived in *North, 1975*, the appropriate value of S is $1 - 0.241(3x^2 - 1)$.

Outgoing radiation from the atmosphere, M, is represented by the linear approximation of the Stefan-Boltzmann law, where A_0 and B_0 are the slope and intercept, respectively, and T is temperature. The Stefan-Boltzmann law describes the relationship between a blackbody's temperature and the energy it radiates per unit surface area per unit time, as given by

$$j^* = \sigma T^4 \tag{3.2}$$

where j^* is the blackbody radiation emissivity, T is temperature, and σ is the Stefan-Boltzmann constant, 5.67×10^8 Wm^{-2}K^{-4}.

To identify this linear estimation function, we use an ordinary least squares regression to minimize the sum of squared differences between the fourth-order Stefan-Boltzmann law and the best linear approximation. The model is first calibrated on Earth parameters before being extrapolated to Titan. We know that Earth's true surface temperature hovers around 288 K, so we identify the range X, between 280 K and 295 K, as an appropriate temperature window within which to examine the behavior of the linearization. Because outgoing longwave radiation is measured from the top of the atmosphere, the Stefan-Boltzmann law takes the form

$$j^* = \sigma(X - 30)^4 \tag{3.3}$$

where the temperature offset of 30 K accounts for the temperature difference between the surface and the top of the troposphere, which is around 30 K colder due to the greenhouse effect in the lower atmosphere. This process yields an M term for Earth of

$$M_E \simeq -857.69 + 3.85T.$$

Before applying this same process to Titan, we first calculate its atmospheric temperature offset by finding the equilibrium temperature for the top of the atmosphere, at which incoming insolation is balanced by outgoing longwave radiation. This equilibrium is defined by setting the cross-sectional insolation profile received by Titan — the global average insolation constant multiplied by one minus the albedo, to define the amount of insolation not reflected — to the full Stefan-Boltzmann law.

$$Q_0(1 - \alpha) = \sigma T^4 \tag{3.4}$$

Solving for T yields a value of approximately 85 K, the equilibrium temperature at the top of the troposphere. Titan's surface temperature ranges between 92 and 93 K; if we take this value to be 92.5 K, the temperature offset is 7.5 K. Initializing an exploratory temperature range of 88 to 98 K yields an M expression for Titan of

$$M_T \simeq -9.93 + 0.14T.$$

Figure 3.1 shows the linearized fits for both Earth and Titan.

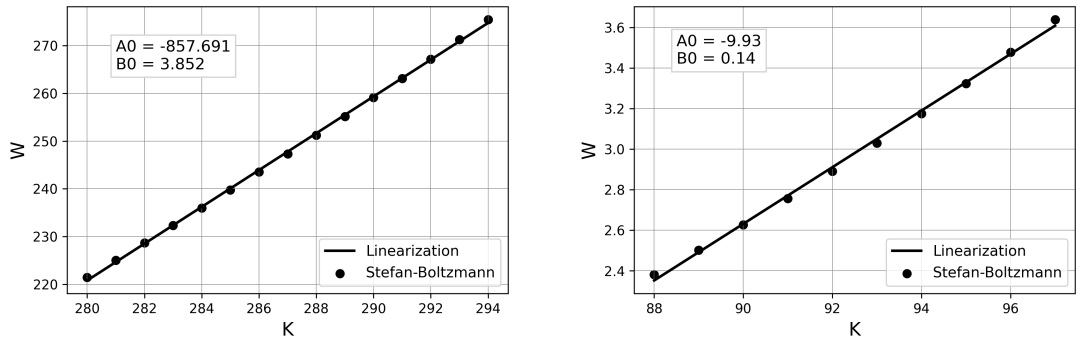

(a) Earth (b) Titan

Figure 3.1: The linearization of the Stefan-Boltzmann law of emittance for Earth and Titan. Earth's temperature range runs from 280 to 295 K for a true surface temperature of 288 K and an equilibrium temperature of 258 K. Titan's temperature range runs from 88 to 98 K for a true surface temperature of approximately 92.5 K and an atmospheric offset of 7.5 K.

3.2 Hydrological Function

The output of the EBM function feeds into the hydrological function, the main tool for computing moist static energy, net precipitation, and latent heat flux, among other quantities that provide a more complete characterization of climate. Following expressions defined in *Siler et al., 2018* [97], the hydrological function uses the moist static energy flux to parameterize global moisture transport based on the data outputted by the EBM function.

The expression for moist static energy flux is given by

$$F(x) = \frac{-2\pi p_0}{g} D(1-x^2)\frac{dh}{dx} \tag{3.5}$$

where p_0 is the reference surface pressure, g the acceleration due to gravity, and D the diffusion coefficient for turbulent diffusivity. The expression $1-x^2$ accounts for a body's spherical geometry, with x as the sine of latitude, and the differential $\frac{dh}{dx}$ evaluates the rate of change of moist static energy globally across space.

Previously, we defined moist static energy to be composed of three terms, including one that denoted the potential energy of a hypothetical parcel of air raised adiabatically through the atmosphere. Because this model does not take into account atmospheric height or layering, the moist static energy expression is modified to

$$h = c_p T + L_v q. \tag{3.6}$$

The specific humidity q is dependent on temperature,

$$q = \frac{RHw}{p_o} e_0 exp\left(\frac{aT}{b+T}\right) \tag{3.7}$$

and relates moisture to the saturation pressure of atmospheric gases. The relative humidity RH is defined as a function. For initial testing and the sake of homogeneity in control simulations, Titan's relative humidity is assumed to be a constant 0.5, but the implementation of a flexible relative humidity function permits sensitivity testing with an array of feasible relative humidity profiles.

The saturation vapor pressure of water vapor on Earth and methane on Titan is represented by the constant value e_0, but the full approximation relating vapor pressure to temperature is given by $e_0 exp\left(\frac{aT}{b+T}\right)$, a formulation of the Clausius-Clapeyron relation, which is a differential equation that characterizes the relationship between pressure and temperature as a substance transitions between phases. The vaporization curves for many substances are mathematical models defining pressure as a function of temperature; they typically exhibit sharply-climbing curves coupling a rise in pressure to an increase in temperature. Experiments have shown that the two quantities are related by

$$P \propto -exp\left(\frac{L_v}{RT}\right)$$

where R is the generalized gas constant 8.31 J mol^{-1} K^{-1} and L_v is the latent heat of vaporization. This expression can be coerced into a form specific to the meteorological implications of liquid water and water vapor,

$$\frac{1}{e_s}\frac{de_s}{dT} = \frac{L_v}{R_v T^2}. \tag{3.8}$$

When integrated, this expression yields the vaporization curve for water vapor widely used in studies of climate and weather. The most common form is the approximation made by *Bolton, 1980* [98], accurate to 0.3% for temperatures between -35 and 35 degrees Celsius,

$$e_s(T) = e_0 exp\left(\frac{aT}{b+T}\right) \tag{3.9}$$

where $a = 17.67$ and $b = 243.5$°C. Given that these values correspond to a temperature in Celsius and our model is coded in SI base units of Kelvin, we undertook another fitting process to derive the Kelvin values of a and b both for water vapor on Earth and methane on Titan. Using a curve fit function, we first confirmed the soundness of the algorithmic process by re-deriving the Celsius values for Earth. Having ensured that our approximation

technique successfully reproduced the same values for a and b obtained by Bolton, we shifted the temperature scale to the appropriate Earth range, between 280 and 295 K, and re-derived the pressure-temperature relationship before doing the same for Titan, changing parameters to accommodate methane rather than water. The curve-fitting results and the values obtained for the parameters are shown in Figure 3.2.

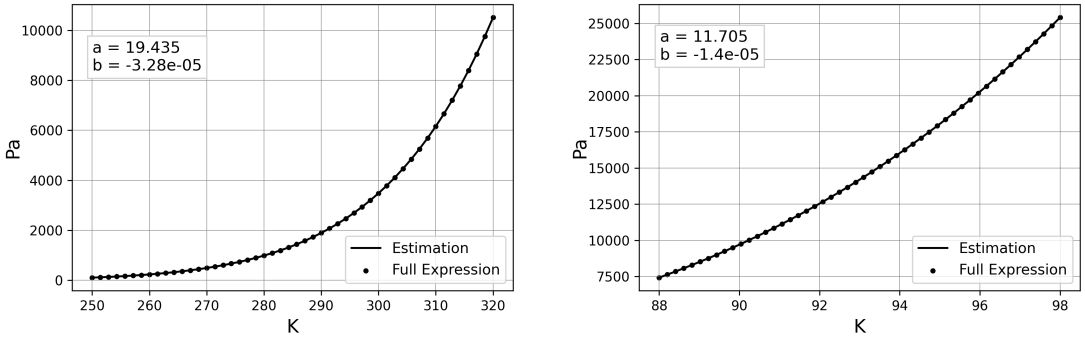

(a) Earth (H_2O) (b) Titan (CH_4)

Figure 3.2: Curve-fitting for the pressure-temperature vaporization curves of water vapor on Earth and methane on Titan over relevant planetary temperature ranges.

With these derived values, we are able to complete the hydrological function and produce graphical outputs of global patterns of temperature, moisture, and energy. We define a weighting function $w(x)$ to partition the effects of the Hadley cell and high-latitude eddies within global circulation,

$$w(x) = 1 - exp\left(\frac{-x^2}{\sigma^2}\right) \tag{3.10}$$

where σ represents the Hadley cell extent, an unknown parameter for Titan. Using this partitioning, we can define the moist static energy flux due to the Hadley cell,

$$F_{HC}(x) = [1 - w(x)]F(x). \tag{3.11}$$

The maximum value of moist static energy is found at the equator; this value can be multiplied by a coefficient λ to yield Γ, the *gross moist stability*, which is a measure of the efficiency of convection at transporting moisture and moist static energy.

$$\Gamma = \lambda h_{max} \tag{3.12}$$

Defining the gross moist stability allows us to formulate the total mass transport of vapor for which the Hadley cell is responsible,

$$V_H = \frac{F_{HC}(x)}{h_{max} + \Gamma - h} \tag{3.13}$$

and, subsequently, the latent heat flux for which the Hadley cell is responsible

$$L_{HC} = -L_v V_H q. \tag{3.14}$$

Latent heat flux comprises a critical component of the planetary energy budget as the flux from surface to atmosphere of energy associated with surface evaporation and tropospheric condensation. Summing the latent heat flux due to the Hadley cell with that transported by eddies, we obtain the total latent heat flux L and can calculate its divergence,

$$\nabla \cdot \vec{L} = \frac{1}{2\pi R^2} \frac{d\vec{L}}{dx}. \tag{3.15}$$

Finally, we use this divergence to calculate the net annual precipitation, evaporation minus precipitation.

$$E - P = 10^6 \pi \frac{\nabla \cdot \vec{L}}{L_v \rho} \tag{3.16}$$

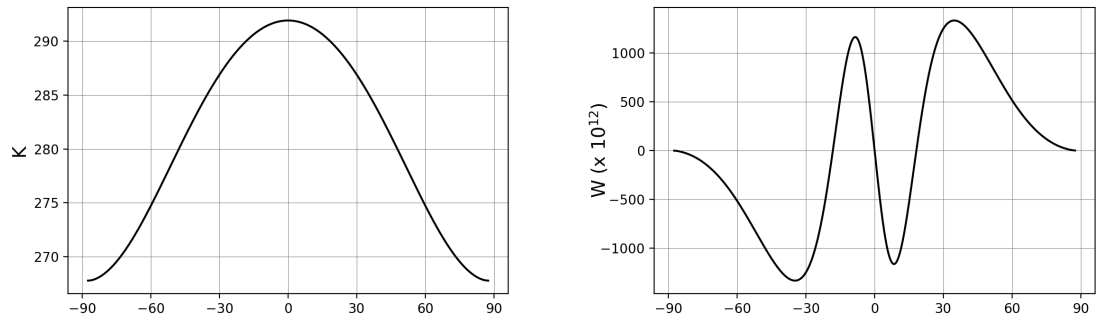

(a) Temperature

(b) Latent heat flux

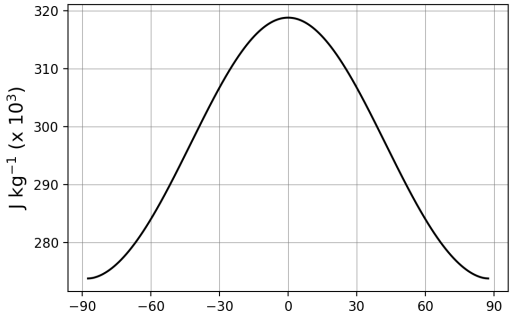

(c) Moist static energy

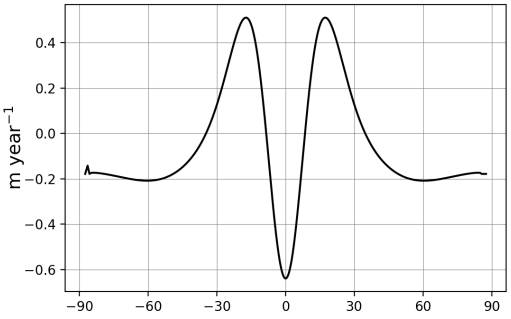

(d) Evaporation minus precipitation

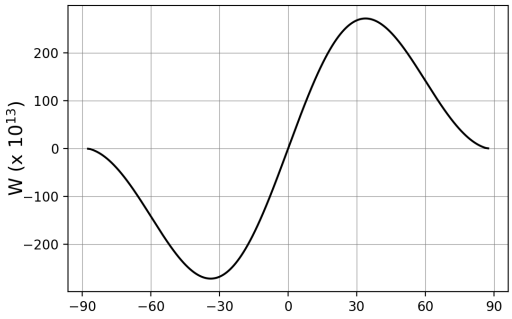

(e) Moist static energy flux

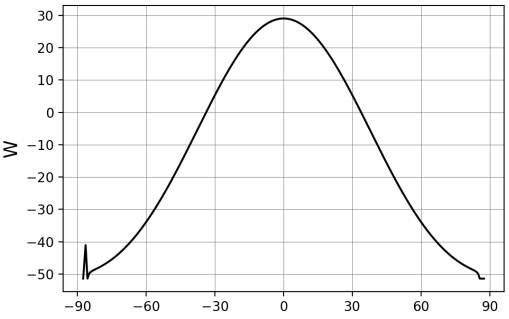

(f) Moist static energy flux divergence

Figure 3.3: Hydrological results for Earth by latitude.

The hydrological function outputs all of these diagnostic quantities: temperature, latent heat flux, net precipitation, and moist static energy as well as its flux and divergence. We find that the values plotted in Figure 3.3 agree well with results from other simulations;

for reference, see *Siler et al., 2018* [97]. The temperature curve is slightly constricted: true average values may be a few Kelvin warmer near the equator and a few Kelvin cooler near the poles. This slight disparity may be the result of assuming a globally constant albedo — other models tend to partition Earth's albedo globally based on surface cover — or taking the temperature offset defined in the insolation linearization to be 30 degrees. This accepted value is an average across the entire surface and troposphere, and is subject to variation.

Examining the other diagnostic plots, we identify trends consistent with what we should expect for latitudinal variation in Earth's weather patterns. Latent energy is a measure of the energy transferred from the surface, specifically the ocean, to the atmosphere. Insolation is strongest at low, equatorial latitudes, where buoyant air is free to rise, constituting one branch of the Hadley cell. We should expect to observe a peak in moist static energy at these latitudes. Accordingly, moist static energy flux describes the poleward flow of this energy, and we find the anticipated peak at the tropical latitudes. Flux diminishes to zero at the poles themselves, as observed on Earth.

Latent heat flux describes energetic flux from surface to atmosphere, and once more we expect to find peaks where we know surface-atmosphere fluxes to take place. Sharp peaks occur within the ICTZ, where precipitation is strongest, as well as at the extratropical latitudes, where extratropical circulation induces condensation and phase transition. Net precipitation points to similar patterns of moisture dispersal. Positive values indicate net drying, while negative values denote surface moisture accumulation. We find the convergence of the Hadley cell at the equator produces heavy annual precipitation. Just beyond this latitude, net drying in the subtropics reflects vertical uptake of the air that powers convection. As expected, precipitation dominates at the mid and polar latitudes. Note that the plot of moisture captures an annual average, negating seasonal effects that might induce a greater degree of asymmetry under particular orbital conditions or on different timescales.

Chapter 4

Results

4.1 Sensitivity Tests

Having calibrated the model to align with known results for Earth, we can confidently apply its framework to Titan in order to investigate analogous climatic properties and patterns. A number of parameters known for Earth are unconfirmed for Titan; these must be estimated and their impacts within the model tested in order to construct the best possible representation of Titan's climate. Outstanding parameters include the diffusion coefficient D, the coefficient of gross moist stability λ, the latitudinal extent of the Hadley cell σ, and the global relative humidity profile RH. Relative humidity has been shown by *Lora & Ádámkovics, 2017* [95] to be decidedly non-constant, following an approximately sinusoidal trend that dips to a minimum of just above 0.5 at low latitudes and rises nearly to 1 at the moisture-rich poles. Later in this section we attempt to replicate this profile prior to building a function which shows that the relative humidity profile converges naturally to that same expected shape when initialized as a global constant.

We begin testing the sensitivity of unknown parameters by initializing a baseline model for Titan. The parameter guesses, shown in Table 4.1, are based either on local values extrapolated globally or estimates from known characteristics of Titan's climate. For each parameter tested, we define a range of reasonable values around the baseline and run the model with each, overlaying diagnostic plots of selected results in order to visualize the degree to which the model is sensitive to change.

Parameter	**Titan Baseline Value**	**Units**
σ	0.6	unitless
λ	1.06	unitless
D	2000	$m^2\ s^{-1}$
RH	0.5	unitless

Table 4.1: Baseline estimations of parameters whose true values are unknown for Titan.

Figure 4.1 shows the plots for the Titan baseline model, revealing some notable differences from the Earth model that are in line with Titan's climatic behavior. Notably, we find that the scales and values for moist static energy and its flux are both vastly different from those associated with Earth. Moist static energy is measured only near the surface as opposed to through the entire vertical extent of Titan's thick atmosphere, meaning these values disagree with those identified by more complex GCM simulations.

We also observe a different pattern of net precipitation that follows Titan's surface distribution of moisture. The low and mid latitudes receive little precipitation, and as expected we find that evaporative processes dominate nearly the entire equatorial range.

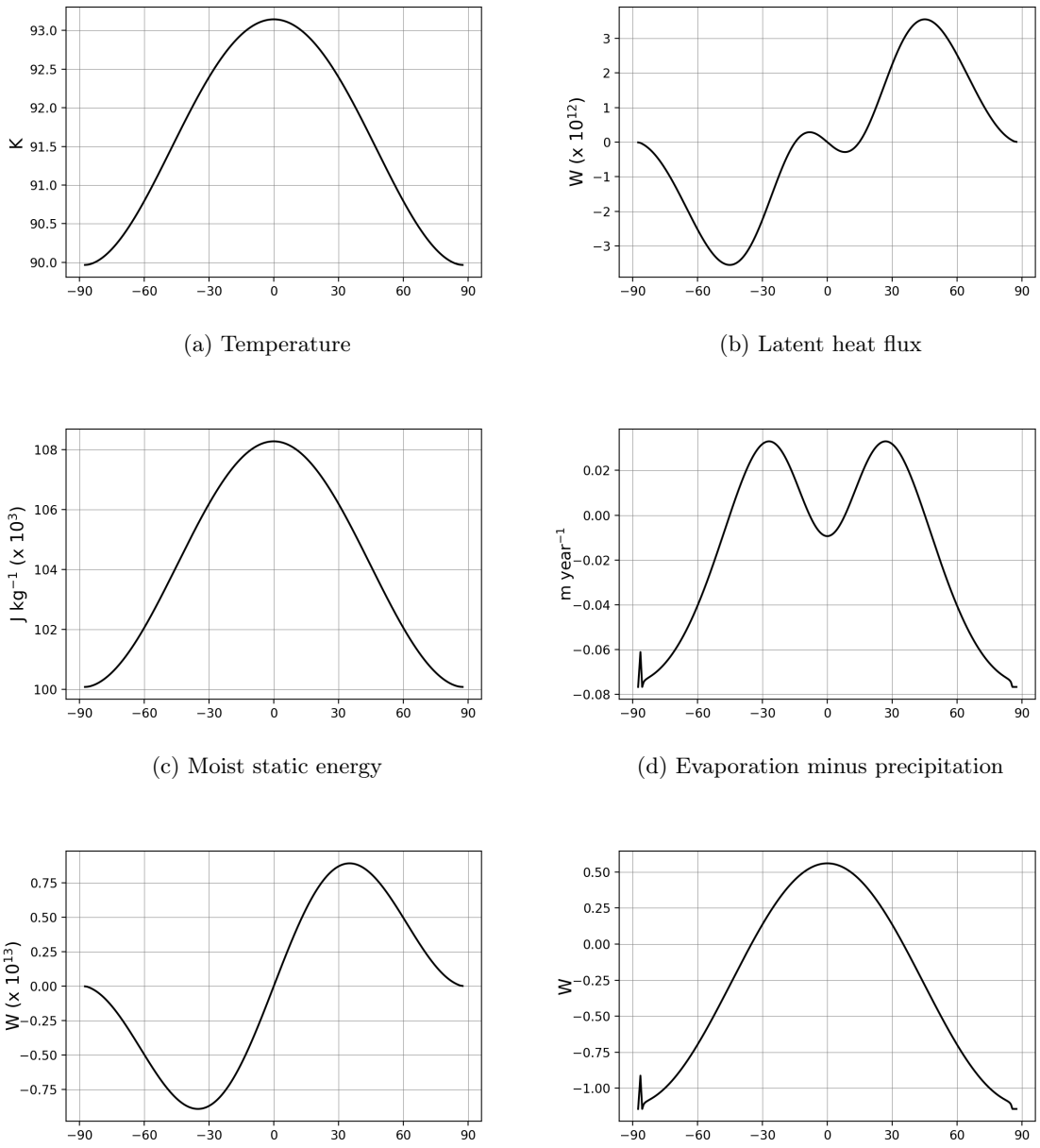

(a) Temperature

(b) Latent heat flux

(c) Moist static energy

(d) Evaporation minus precipitation

(e) Moist static energy flux

(f) Moist static energy flux divergence

Figure 4.1: Hydrological results for Titan by latitude, with default parameters shown in Table 4.1, including a globally constant relative humidity. Note the differences and similarities with Earth's defaults. Temperature (4.1a) and moist static energy (4.1c) peak at the equator, albeit at different scales, and net precipitation (4.1d) reflects observed moisture-rich poles.

In contrast to Earth, where processes of precipitation lead to only moderate accumulation at the poles, we find for Titan that the global maximum of wetting arises at high latitudes, in line with the moon's polar concentration of surface liquid. The scale of net precipitation received on Titan is roughly an order of magnitude lower than that of Earth.

4.1.1 Sigma

The σ value is tested between 0.3 and 0.9 in steps of 0.1. These values correspond to Hadley cell extents that only cover low latitudes as well as those stretching to the poles. Of the four parameters whose sensitivities are tested, the true value of σ is the most straightforward to estimate. On Earth, this value is 0.3, meaning that Hadley cell effects dominate until roughly 30 degrees latitude in each hemisphere, at which point eddy effects assume control as the driving force behind circulation. The same principle should hold for Titan, which is known to feature eddy effects that have emerged organically in model simulations [91], but these eddy effects should not dominate until around 55 or 60 degrees latitude. Plotting for different values the weighting function $w(x)$, a simple Gaussian curve which partitions the effects of the Hadley cell and the effects of eddies, allows a simple visual approximation to be made. A good estimation for σ is the latitude where $w(x)$ shows that Hadley cell effects in the overall transport of energy go to zero.

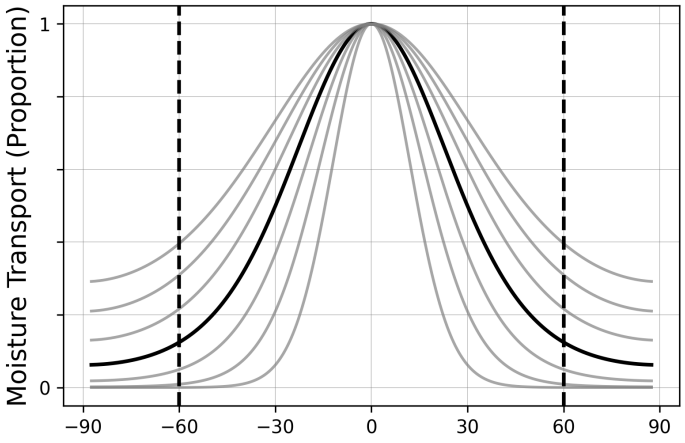

Figure 4.2: The weighting function $w(x)$, plotted for different values of σ beween 0.3 and 0.9. The black line represents $\sigma = 0.6$, considered the best estimation for the true value. Dotted vertical lines mark the latitudinal boundary where Hadley cell effects governing moisture transport should taper off as the influence of polar eddies dominates.

Using a rough estimation of $\sigma = 0.6$ as a baseline for comparison, the model is run for each of the sigma values and its diagnostic plots analyzed. The only substantial changes due to σ fluctuation are found for net precipitation and latent heat, two related aspects of climate. Figure 4.3 shows these results. We find that as σ increases, the global distribution of moisture becomes more uniform as precipitation and moisture transport become less concentrated in latitudinal extremes. The peaks in latent heat in each hemisphere are less pronounced for $\sigma = 0.9$, since moisture and energy are dispersed over a greater latitudinal extent as compared to the case when $\sigma = 0.3$, and they appear to 'migrate' toward the poles — as σ rises, peaks are achieved at more poleward latitudes, once more reflecting a wider latitudinal footprint. We also find a similar flattening of net precipitation across the global expanse: the entire profile is more extreme for lower σ values, with higher peaks of net drying in the subtropics and moisture accumulation at the poles. These peaks are suppressed as σ rises to 0.9.

Despite the observed differences in model results due to the adjustment of σ, the parameter does not appear to have too strong an effect on the global climate system at large. All iterations of σ result in profiles of net precipitation and latent heat flux that converge to the same value at equatorial latitudes. For net precipitation, the differences at

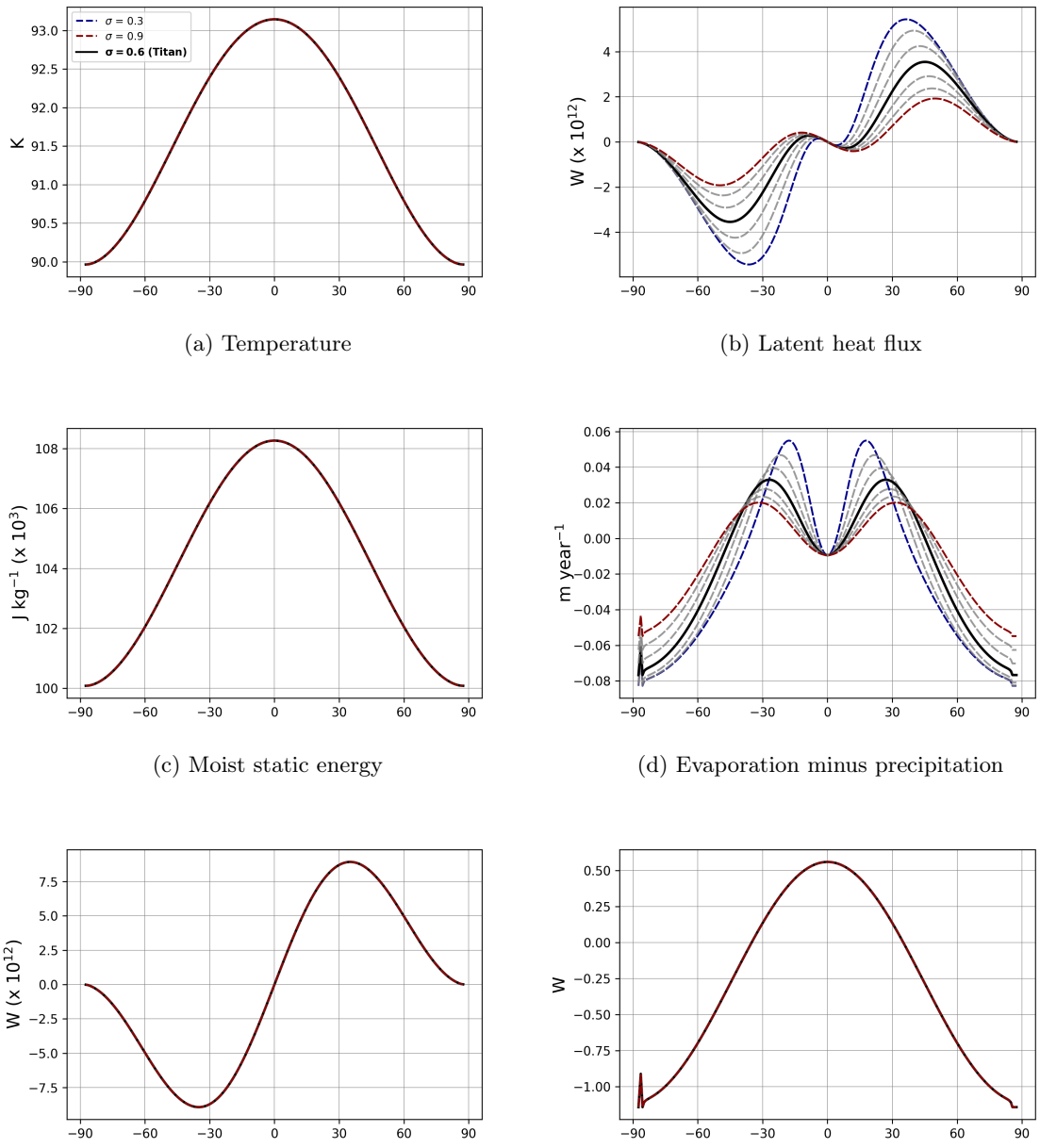

(a) Temperature

(b) Latent heat flux

(c) Moist static energy

(d) Evaporation minus precipitation

(e) Moist static energy flux

(f) Moist static energy flux divergence

Figure 4.3: Hydrological outputs for sensitivity tests of σ. Only latent heat flux (4.3b) and net precipitation (4.3d) appear to be affected by changes to the Hadley cell extent. At higher σ values, we observe suppressed and poleward-trending peaks in latent flux, as well as less-pronounced extremes in both sub-tropical surface drying and polar surface wetting.

tropical and polar latitudes are not overly pronounced — just a few centimeters of variance in rainfall each year. Latent heat flux varies more drastically, as the same budget of energy is dispersed across a wider latitudinal band. Overall, though, the extent of the Hadley cell does not appear to be a property of the climate system that radically alters its behavior, likely due to its role more as a feature moderating the scale of climatic processes rather than controlling their very nature.

4.1.2 Lambda

We next turn to λ, the coefficient of gross moist stability, a measure of the efficiency of moisture transport in convective processes and a key component of the expressions for latent heat flux and net precipitation. The full expression for gross moist stability is given by Equation 3.12 as the maximum value of moist static energy, multiplied by some λ tuning coefficient. The baseline value of λ cited in *Siler et al., 2018* [97] is 1.06. We test the model for values between 0.25 and 2 in steps of 0.25 and compare the results with those of the baseline.

Figure 4.4 reveals that greater gross moist stability results in more uniform latitudinal distribution of moisture and energy. A λ value of just 0.25 produces net precipitation at equatorial and polar latitudes, as well as greater latent energy fluxes in the subtropics, in a profile similar to that found on Earth. A higher λ corresponds to net drying across a wide band of non-polar latitudes and, subsequently, lower latent heat fluxes associated with surface-atmosphere energy transfer. It appears that gross moist stability, as a measure of efficiency in convective processes, serves to 'smooth' global moisture distribution: lower gross moist stability allows moisture to be collected predominantly at certain latitudes, while higher values permit moisture to carry toward the poles and spread more uniformly across all latitudes.

Though inappropriate to directly compare, examining these results relative to those generated by more complex GCMs can help discern an appropriate λ value. GCM outputs like those depicted in *Lora et al., 2014* [34] reveal a greater vertical range of latent heat flux values and more pronounced latent heat flux peaks around equatorial latitudes. The true coefficient of gross moist stability likely strays from the approximation of 1.06, but further work would be necessary to determine the optimal λ value for this EBM and how it translates to more granular GCM climate approximations.

4.1.3 Diffusivity

The diffusion coefficient, D, governs the parameter of turbulent mixing. The Earth value is approximately 1.16×10^6 $\mathrm{m^2 s^{-1}}$, a constant that was fit to Earth's zonal mean temperature profile from nearly 20 years of simulations. As in previous studies, D is assumed to be latitudinally uniform.

Testing this parameter's sensitivity to better understand its behavior and influence was inspired by a failure to discern a reasonable Titan value based on prior work. Initially, we sought to re-derive a Titan-specific value for D with the formula put forth by *Williams & Kasting, 1997* [99]:

$$\left(\frac{D}{D_0}\right) = \left(\frac{p}{p_0}\right)\left(\frac{c_p}{c_{p0}}\right)\left(\frac{m_0}{m}\right)^2\left(\frac{\Omega_0}{\Omega}\right)^2 \tag{4.1}$$

This expression is generalizable, meaning each term is expressed relative to its equivalent on Earth. D is the diffusion coefficient we attempt to derive; p is the reference surface pressure; c_p is the specific heat; m is the mean molecular mass, or the average atomic mass of the atmosphere based on its composition; Ω is the planetary rotation rate — in Titan's case, the rate at which it orbits Saturn. All subscript values denote Earth parameters.

This method, incorporating the known value of D_0, yielded a diffusion coefficient for Titan that was conspicuously high and proceeded to break the model, generating physically nonsensical results. These included inverted distributions of temperature, where the poles were warmer than the equator, as well as temperature gradients between the global maximum and minimum on the unrealistically small order of 10^{-5}. Realizing that the assumptions of this method rendered it unfit to estimate the diffusion coefficient on Titan,

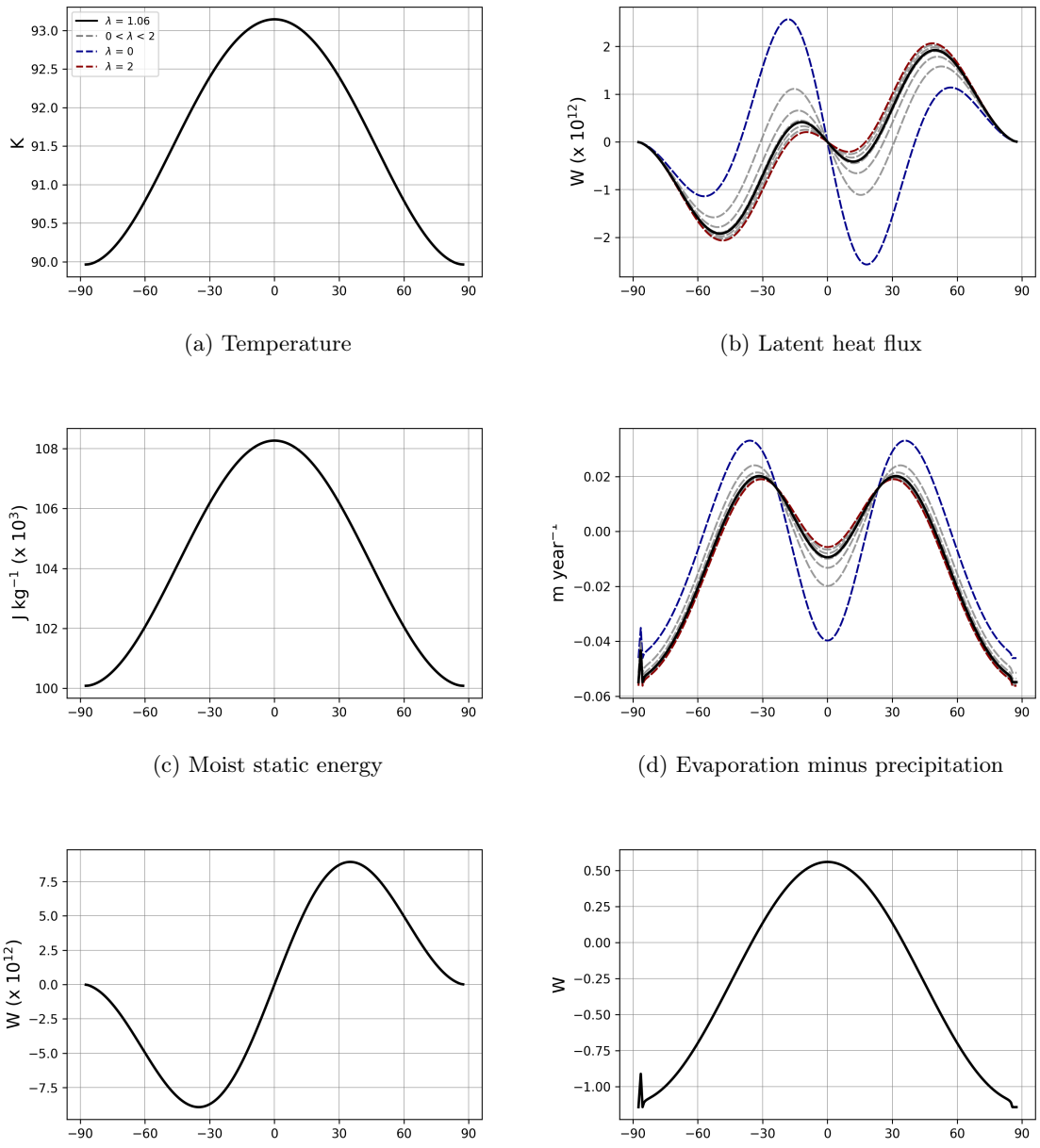

(a) Temperature

(b) Latent heat flux

(c) Moist static energy

(d) Evaporation minus precipitation

(e) Moist static energy flux

(f) Moist static energy flux divergence

Figure 4.4: Hydrological outputs for sensitivity tests of λ. We find that higher values lead to more Earth-like profiles of latent heat flux and net precipitation across the equatorial latitudes. The profile of latent heat flux (4.4b) is more in line with GCM simulations at lower values of λ, suggesting that 1.06 is not a great approximation. These lower values, however, are more likely to result in net equatorial wetting, as shown by the blue curve in (4.4d), an unrealistic phenomenon on Titan. Further exploration and more sensitive testing would be required to balance these competing effects.

we engaged in sensitivity testing to ultimately fit the parameter to match known profiles of temperature and energy.

Testing D values that range between 200 and 10^4 reveals that the parameter affects all hydrological outputs. The value of D generated by the *Williams & Kasting, 1997* approximation was on the order of 10^8, but we find negligible differences between the

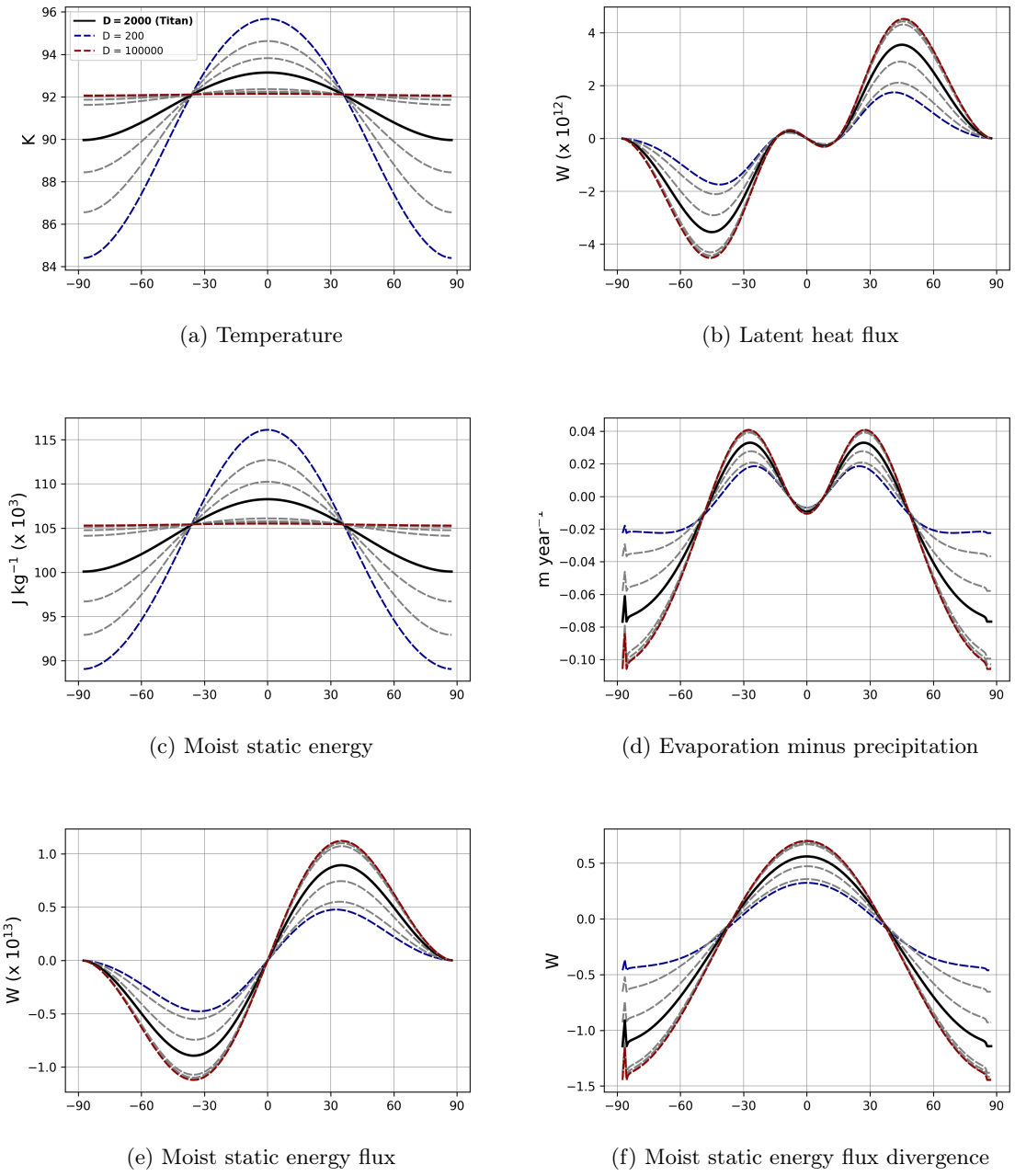

(a) Temperature

(b) Latent heat flux

(c) Moist static energy

(d) Evaporation minus precipitation

(e) Moist static energy flux

(f) Moist static energy flux divergence

Figure 4.5: Hydrological outputs for sensitivity tests of D, the diffusion coefficient. The temperature (4.5a) and moist static energy (4.5c) curves produced by different values of D serve as helpful constraints in understanding the parameter's true scale. The D that produces the most appropriate temperature and moist static energy curves is on the order of 10^3, confirming that the *Williams & Kasting, 1997* approximation on the order of 10^8 was far too high.

model's performance at this value and at 10^4.

The results show that higher values of D flatten the range of both temperature and moist static energy while widening that of the other hydrological outputs. This testing allows us to identify the best value for D as around 2,000; we find that the temperature range associated with this value is the best match for Titan's observed temperature range, 2–3 K between equator and pole. In contrast to temperature and moist static energy,

distributions of both latent heat flux and net precipitation assume the same profile at equatorial latitudes, no matter the value of D. Changes to these distributions are evident at the mid latitudes and poles, respectively, whereas variance in D appears to alter the profiles of temperature and moist static energy at nearly all latitudes.

4.1.4 Relative Humidity

Finally, we probe the sensitivity of Titan's relative humidity profile and build a recursive function to examine whether the model is able to naturally converge to a known solution for relative humidity and net precipitation. *Lora & Ádámkovics, 2017* show that Titan's relative humidity profile dips to a global minimum at the arid equatorial latitudes and peaks near 1 at both the poles [95], a finding in line with what we expect based on the polar concentration of surface moisture accumulation. In examining the sensitivity of the model to changes in relative humidity, we attempt to represent the true function underlying this distribution and understand its behavior within the model.

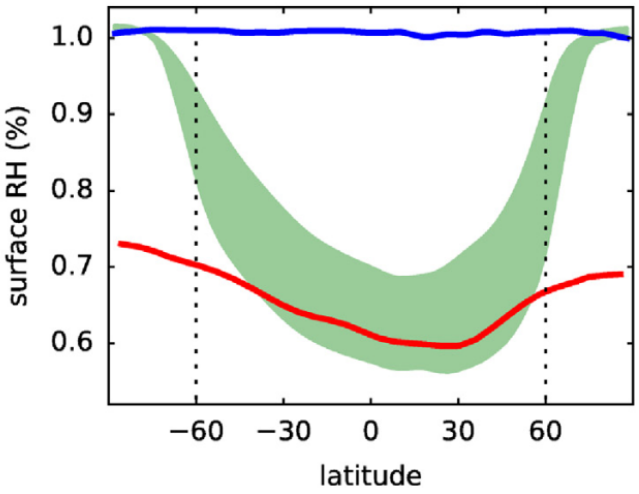

Figure 4.6: The range of simulations approximating Titan's relative humidity profile, represented by the green area, as conducted in *Lora & Ádámkovics, 2017* [95].

Any approximation of the function that underlies the relationship between relative humidity and latitude will be constrained by the results of model simulations. The general shape of the relative humidity profile is known; as such, the function that approximates it can only conform to a certain range of parameters. We see from Figure 4.6 that the plausible range of relative humidity profiles follows an approximately sinusoidal curve. We identify 78 possible expressions of the form

$$RH = F + Acos(Bx)$$

where x is latitude, F is the vertical offset, A is the amplitude, and B is the period. All 78 expressions roughly approximate the curve shown in Figure 4.6, meaning they are constrained to have equatorial minima between 0.5 and 0.7, with polar maxima between 0.9 and 1. These ranges are intentionally set wider than the specifications of Figure 4.6 in order to capture and understand the behavior of as many expressions as possible.

As shown in Figure 4.7, running the model with all 78 of these expressions as the relative humidity approximation yields a mess of plots but provides useful information: only some of the expressions produce meaningful results. Others generate outputs contradictory to observations, such as net annual drying at the poles or moist static energy curves that

are inverted so that polar values exceed those found at the equator. Filtering out these expressions yields 41 that produce meaningful results.

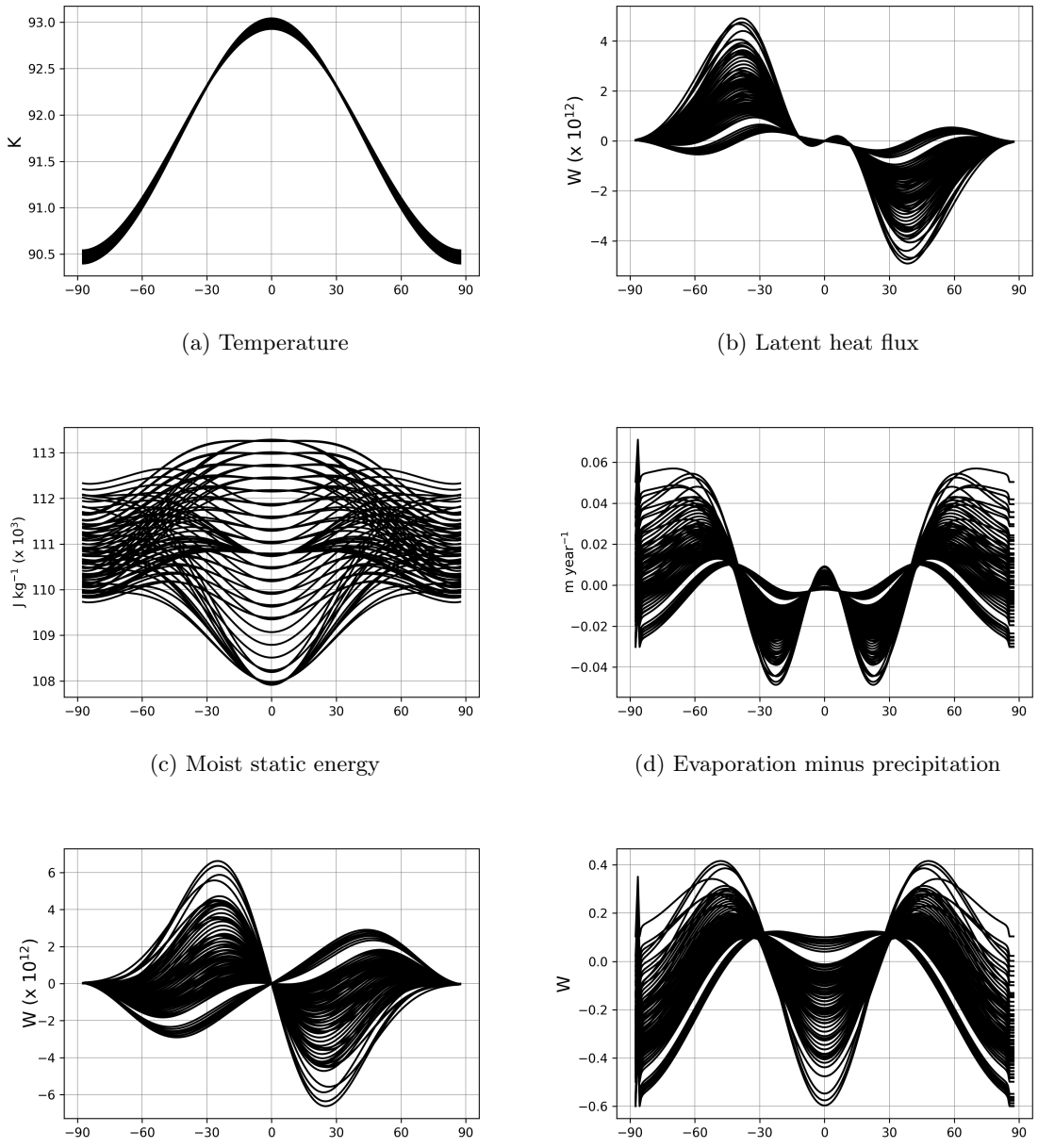

(a) Temperature

(b) Latent heat flux

(c) Moist static energy

(d) Evaporation minus precipitation

(e) Moist static energy flux

(f) Moist static energy flux divergence

Figure 4.7: Hydrological outputs for all 78 feasible expressions for relative humidity that were initially tested. Broad trends can be observed from these plots, namely that although all expressions conform to Titan's known relative humidity profile, only some of them produce meaningful outputs when incorporated into the model.

We then select from this group only the values that strictly conform to the observed relative humidity profile. Initially, polar values of relative humidity were allowed to range between 0.9 and 1, even though simulations [95] suggest the true relative humidity at the highest latitudes is right around 1. Examining the viable expressions, most exhibit polar values of relative humidity that are between 0.9 and 0.95. We attempt to identify expressions with polar values near 1, but no expression yields such values that exceed 0.97,

so we limit the selection to the four expressions above 0.96.

Though there are slight disparities from what is expected, these four expressions produce meaningful results, shown in Figure 4.8. In alignment with observations, the shape of the moist static energy is concave, with a global maximum at equatorial latitudes and a drop-off toward the poles. The profile of net precipitation exhibits more pronounced differences from previous iterations that had a flat relative humidity profile, most notably predicting net moisture accumulation at the low latitudes on either side of the equator. But the overall distribution — featuring net precipitation at the poles and net drying throughout the mid latitudes — matches the expectation for Titan.

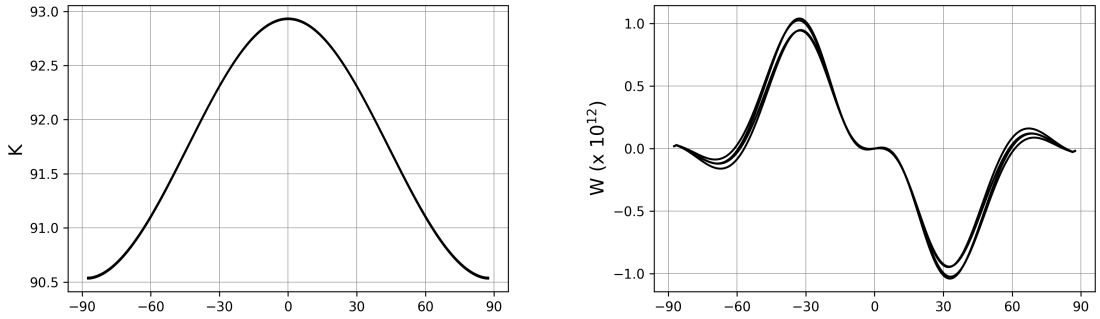

(a) Temperature

(b) Latent heat flux

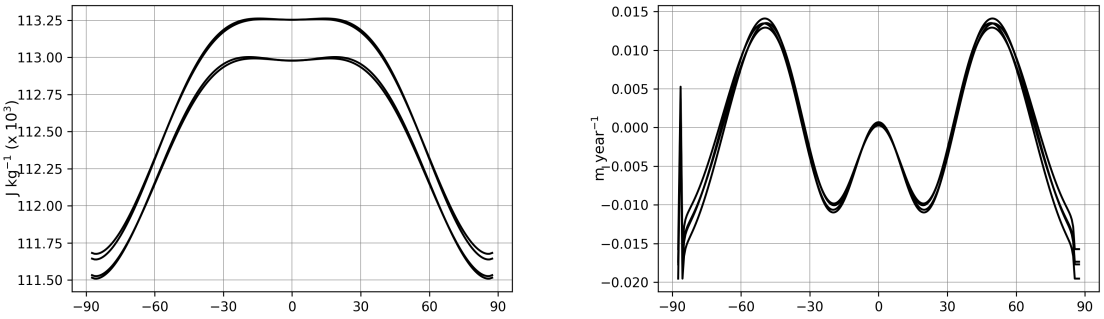

(c) Moist static energy

(d) Evaporation minus precipitation

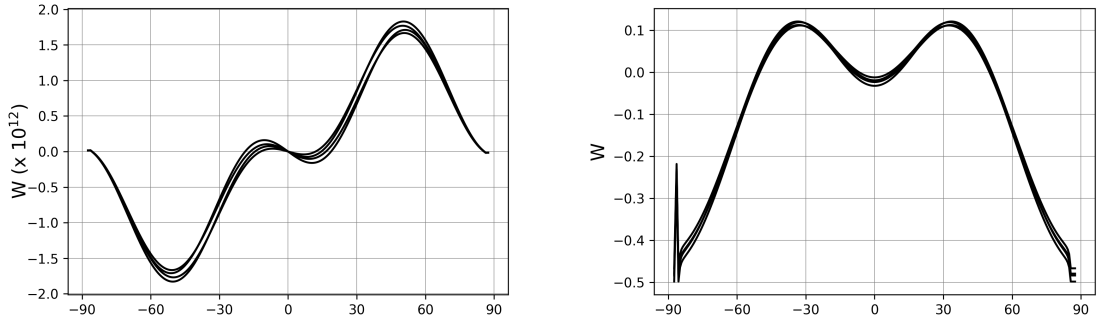

(e) Moist static energy flux

(f) Moist static energy flux divergence

Figure 4.8: Hydrological outputs from the four expressions that most closely match the known relative humidity profile in terms of polar behavior. We find that the variance in parameters of these functions is minute, as shown in Table 4.2, confirming the model's sensitivity to relative humidity input.

Based on these sensitivity tests, the model is extremely sensitive to relative humidity input. Of 78 plausible expressions for relative humidity, only four provide both sensible results for moisture processes and reasonable matches for the posited relative humidity profile on Titan. The parameters of these four expressions, as shown in Table 4.2, are all very similar: we notice that the range of viable values for B and F is just 0.1, while the range of possible A values is a mere 0.01. Only a narrow range of possible expressions produces meaningful results, and the difference between F and the absolute value of A is either 0.71 or 0.72. The fine line between a working model and a nonsensical one indicates that slight deviations from these estimates can drastically affect the system as a whole.

A	B	F	Full Expression
-0.51	1.1	1.2	$1.2 - 0.51cos(1.1xin)$
-0.52	1.1	1.2	$1.2 - 0.52cos(1.1xin)$
-0.61	1	1.3	$1.3 - 0.61cos(xin)$
-0.62	1	1.3	$1.3 - 0.62cos(xin)$

Table 4.2: Best estimates for terms of relative humidity profiles that produce meaningful model results.

More work on this type of testing, coupled with corroboration from observation and from other models, assuredly remains. The sensitivity testing conducted here constitutes only a rough approach: without simulation data, we did not fit expressions to mathematically match the simulated profile as closely as possible, nor did we incorporate the slight hemispheric asymmetry thought to exist. We made a qualitative assessment of the types of expressions that might best capture trends in the data, but in reality the relative humidity is determined by the interactions between complex geological, meteorological, and physical systems that cannot be distilled into a simple sinusoidal approximation. Nonetheless, this crude process permits the approximation of an expression that both mirrors the simulated relative humidity profile and engenders sensible model output from the EBM, thus illuminating some understanding of just how critical and sensitive a climatic component relative humidity may be.

4.2 Recursive Relative Humidity Function

To further explore relative humidity, we create a recursive function that naturally converges to a stable equilibrium of global moisture distribution. The relative humidity profile is initialized as a constant across all latitudes, and two metrics are defined. One, the step metric δ, is the amount by which each iteration of the function is incremented. The other is the function's convergence tracker, measuring the overall change between one iteration and the next. Once this tracker crosses a certain threshold signifying that the result is changing minimally, the function stops and indicates that convergence has been achieved.

With the relative humidity profile initially held constant, the function runs the model and stores the hydrological output for net precipitation across Titan. The relative humidity profile is then updated based on this distribution of moisture across the surface. Relative humidity is higher over liquid than ground cover; accordingly, the relative humidity profile is raised at latitudes where moisture has accumulated and lowered at dry latitudes. The magnitude of these changes is proportional to the current iteration of the net moisture profile, multiplied by the coefficient of the step increment δ.

The result is smoothed and becomes the relative humidity function fed into the next iteration of the model. As a proportion, relative humidity is always bounded between 0 and 1, meaning the relative humidity function is similarly constrained prior to being approxi-

mated by an order-four polynomial. Early attempts to realize this approximation used far more complex polynomials, which led to wildly fluctuating output as these functions were fed back into the model. We found that an order-four approximation was able to both capture the appropriate behavior and lead to a convergent solution.

For reasonable values of δ and the convergence threshold, this feedback function converges to a stable equilibrium of net precipitation and a relative humidity profile that matches known results. This outcome points to the model's robustness and provides insight into how Titan's relative humidity profile settled into the shape that it did. An early aqueous world, for example, with a roughly constant global relative humidity would slowly have evolved under Titan conditions to adopt the presently observed relative humidity profile through an analogous process.

A number of curious aspects of this function remain to be explored. Convergence behavior varies based on the assigned values of δ and the convergence threshold; when δ is large, for example, and alters the relative humidity profile by a multiple of net precipitation greater than 1, the solution spirals into an unstable equilibrium. Diagnostic plots show wild fluctuation across all metrics, including temperature, in behavior similar to that found when overly complex polynomials were fit to the relative humidity profile.

We also find that the function is highly sensitive to initial conditions. Initial profiles of constant relative humidity at different values will lead to starkly different results. Figure 4.9 shows the convergent relative humidity solutions for three varied constant initial profiles. Though their shapes appear to match expectations, these solutions should eventually converge to the same profile; instead, they center themselves around their starting values.

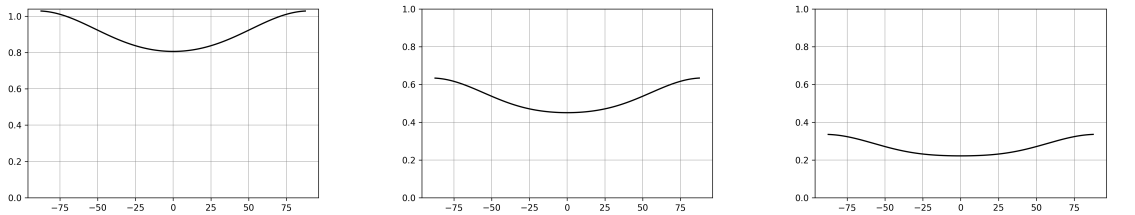

(a) Initial condition $RH_0 = 1$ (b) Initial condition $RH_0 = 0.5$ (c) Initial condition $RH_0 = 0.25$

Figure 4.9: Relative humidity profiles generated by the recursive function for different initial conditions where δ equals 1 and the convergence threshold equals 0.01.

Since relative humidity is not a direct catalyst of climatic processes but a result that emerges from their progression, we look to the underlying nature of the hydrological cycle in an effort to identify the physical mechanisms that may be responsible for this sensitivity to initial conditions. The problem is essentially that polar values of relative humidity are low. Whether they stretch to nearly 1, the value they should reach as surface liquid continues to accumulate at the high latitudes, is dependent on the profile initialized in the function. If relative humidity is initially set at a constant of 1, the desired behavior is achieved. At an initial value of 0.5, however, it is not.

The explanation for this issue may lie in the expression for moist static energy flux divergence, which in turn is predicated on latent heat flux, which involves specific and relative humidity. In the final, convergent iteration of net precipitation, values are not as extreme as we might expect — there is less overall precipitation at the poles. Lower polar values of relative humidity contribute to a self-defeating cycle that perpetuates this type of behavior: lower polar relative humidity means lower specific humidity and latent heat flux, implying that less surface-atmosphere energy transfer is occurring at polar latitudes. Lower latent heat flux corresponds to less intense moisture exchange processes that drive

the accumulation of polar moisture, and less polar moisture engenders relative humidity profiles that are limited in subsequent simulations. It appears necessary to re-balance with each iteration the poleward flow of moisture and energy associated with moist processes, something that may be accomplished with a reworked expression for moist static energy.

The first term of the moist static energy expression denotes internal energy, while the second shows the contribution of moisture. Given that we are accounting only for near-surface moist static energy, a substantial portion of the total moisture contained in the atmosphere is unaccounted for in the model, contributing to an incomplete accumulation of polar moisture at each recursive iteration. A potential solution to the function's sensitivity to initial conditions may emerge from counterbalancing decreases in the relative humidity-based moisture term with some compensation that preserves a better approximation for the true moist static energy profile. The introduction of supplemental moist static energy would influence the behavior of moist static energy flux and mass transport by the Hadley cell, both of which contribute to balancing processes of polar moisture accumulation.

An alternative solution may incorporate seasonal or orbital effects not present in this model, permitting asymmetry and polar moisture to build up over time. Further work is needed to thoroughly investigate the paths by which the climate system achieves stable equilibrium under various circumstances, and introducing a temporal component to the model constitutes an important and potentially revelatory step.

Chapter 5

Discussion

In this project, we have created a one-dimensional energy balance model, calibrated it to successfully capture the climate profile of Earth, and applied it to Titan to better understand the behavior of the moon's climate system and the latitudinal dependencies of its processes of moisture and energy transport. By first providing an overview of Titan's planetary conditions and the framework of its climatic system, the model and its implications can be placed within the proper context. We realize a net solar forcing function that analyzes the balance of incoming and outgoing radiation, then construct atop it a hydrological function outputting the parameters that capture the behavior of the global climate system. In order to understand how the system responds to changes in moisture distribution processes, we take advantage of the model's computational flexibility to conduct sensitivity tests for unknown parameters, including diffusivity and the global profile of relative humidity. Finally, we create a recursive feedback function that updates relative humidity over successive iterations based on the latitudinal profile of surface moisture, finding that the model permits natural convergence to a stable equilibrium that mirrors Titan's observed relative humidity profile. We determine that more work is needed to free the function from its dependence on initial moisture conditions.

This model provides a flexible and powerful starting point for further exploration of Titan's climate system, and there are numerous avenues for continued progress. The field of Titan studies would benefit from an efficient EBM able to illuminate the same broad global trends in weather and climate that are revealed over arduous computational processes by GCMs. Such a tool would give researchers the freedom to adjust parameters to particular theoretical constraints in order to learn about how Titan's climate system would behave, or examine how particular conditions may have shaped the moon's evolution. The first step to these future advances is, indisputably, an expansion of this model. Sensitivity testing and the incorporation of Hadley cell effects form a solid baseline, but the introduction of a temporal component permitting the emergence of seasonal and orbital asymmetry would constitute a crucial advance in marrying computational simplicity with informative climate modeling. Implementing an insolation function dependent on orbital parameters — and, implicitly, on a temporal component corresponding to those parameters — is a logical next step toward this goal. An expression like that found in *Lora et al., 2011* would make sense:

$$S_{ave} = \frac{S_0 E^2}{2\pi} \int_{-h_0}^{h_0} (sin\phi sin\delta + cos\phi cos\delta cosh) e^{-\tau/(sin\phi sin\delta + cos\phi cos\delta cosh)} dh. \tag{5.1}$$

This expression incorporates latitude ϕ with hourly variance in insolation h and solar declination δ alongside other orbital characteristics — eccentricity e, orbital angle Θ and longitude of perihelion ϖ are contained within the full expression for E. Along with others, Alexander Hayes of Cornell has compiled a collection of orbital data calculated

for thousands of years of Titan's past. This type of data would form the backbone of an expanded model conducive to studying Titan's hemispheric asymmetries.

Further steps include imposing more constraints on unknown parameters in order to pinpoint their true values. Our sensitivity tests utilize the model's flexibility to understand how the climate system behaves when such parameters are adjusted within a specific range, but they do a poor job of narrowing in on optimal values or ranges that best align with the physical processes observed on Titan. Identifying the true nature of these parameters would require corroboration with observational data and other climate models, but could open up new possibilities for probing the climate system with EBMs.

Acknowledgments

The author thanks Juan M. Lora of the Yale University Department of Earth and Planetary Sciences for his continued guidance, vision, and patient encouragement throughout the research and model-building processes, even as they meandered between various ideas and potential outcomes. Thanks to Prof. Lora and Virginia Archambault for their feedback on the scientific and narrative quality of this paper.

The author also thanks Alexander Hayes of Cornell University, Nick Siler of Oregon State University, Tyler Kukla of Stanford University, and Daniel Ibarra of Brown University for their time and assistance in providing source code and other helpful resources.

Statement of Contributions

The theoretical basis and idea for this project were conceived by Nicholas James Archambault, Yale University class of 2021, independent from Juan M. Lora or the influence of any member of the Lora research group. All aspects of model creation, testing, and generalization were completed solely by N.J.A. The review of Titan literature and the crafting of this paper were conducted independently by N.J.A., with helpful edits provided by J.M.L.

While J.M.L. lent guidance on general structure and scope, this project is fully attributable to N.J.A.; in no way does it constitute a continuation or direct extension of ongoing work by either J.M.L. or any member of the Lora group.

Bibliography

[1] S.M. Horst. Titan's atmosphere and climate. *Journal of Geophysical Research: Planets*, 122, Mar 2017.

[2] Nasa's Dragonfly will fly around Titan looking for origins, signs of life. *NASA*, Jun 2019.

[3] G.P. Kuiper. Titan: a satellite with an atmosphere. *Astrophysical Journal*, 100:378–383, Apr 1944.

[4] A.L. Broadfoot et al. Extreme ultraviolet observations from Voyager 1 encounter with Titan. *Science*, 212:206–211, Apr 1981.

[5] G.F. Lindal et al. The atmosphere of Titan: An analysis of the Voyager 1 radio occultation measurements. *Icarus*, 53:348–363, Feb 1983.

[6] D.M. Hunten et al. *Titan.* University of Arizona Press, Tucson, Arizona, 1984.

[7] R. Lopes et al. Titan as revealed by the Cassini radar. *Space Science Reviews*, 215, May 2019.

[8] Science highlights from Huygens. *European Space Agency*, Sep 2019.

[9] H.B. Niemann et al. Composition of Titan's lower atmosphere and simple surface volatiles as measured by the Cassini-Huygens probe gas chromatograph mass spectrometer experiment. *Journal of Geophysical Research: Planets*, 115, Dec 2010.

[10] V.G. Kunde et al. C_4H_2, HC_3N, and C_2H_4 in Titan's atmosphere. *Nature*, 292:686–688, Aug 1981.

[11] R.L. Samuelson et al. Mean molecular weight and hydrogen abundance of Titan's atmosphere. *Nature*, 292:688–693, Aug 1981.

[12] V. Vuitton et al. Ion chemistry and N-containing molecules in Titan's upper atmosphere. *Icarus*, 191:722–742, Aug 2007.

[13] M. Fulchignoni, F. Ferri, et al. *In situ* measurements of the physical characteristics of Titan's environment. *Nature*, 438:785–791, Nov 2005.

[14] M. Fulchignoni, F. Ferri, et al. *Huygens ASI measurements at Titan: an insight of Titan's atmosphere and surface.* 2015.

[15] G.H. Roe et al. The remote impacts of climate feedbacks on regional climate predictability. *Nature Geoscience*, 8:135–139, Jan 2015.

[16] C.A. Griffith et al. Radiative transfer analyses of Titan's tropical atmosphere. *Icarus*, 218:975–988, Apr 2012.

[17] D.F. Strobel. The photochemistry of hydrocarbons in the atmosphere of Titan. *Icarus*, 21:785–791, 1974.

[18] M. Strobel, Y.L. Yung, and J.P. Pinto. Titan—Aerosol photochemistry and variations related to the sunspot cycle. *Astrophysical Journal*, 242:125–128, 1980.

[19] S.K. Atreya, T.M. Donahue, and W.R. Kuhn. Evolution of a nitrogen atmosphere on Titan. *Science*, 201:611–613, Aug 1978.

[20] C. Li et al. A non-monotonic eddy diffusivity profile of Titan's atmosphere revealed by Cassini observations. *Planetary Space Science*, 104:48–58, 2014.

[21] K.E. Mandt et al. The $^{12}C/^{13}C$ ratio on Titan from Cassini INMS measurements and implications for the evolution of methane. *Astrophysical Journal*, 749:48–58, 2012.

[22] P. Lavvas et al. Energy deposition and primary chemical products in Titan's upper atmosphere. *Icarus*, 213:233–251, May 2011.

[23] Y.L. Yung et al. Photochemistry of the atmosphere of Titan: comparison between model and observations. *Astrophysical Journal*, 55, Jul 1984.

[24] B.L. Lutz et al. Titan: Discovery of carbon monoxide in its atmosphere. *Science*, 220:1374–1375, Jun 1983.

[25] R.E. Hartle et al. Preliminary interpretation of Titan plasma interaction as observed by the Cassini Plasma Spectrometer: Comparisons with Voyager 1. *Geophysical Research Letters*, 3, Apr 2006.

[26] S.M. Horst, V. Vuitton, and R.V. Yelle. Origin of oxygen species in Titan's atmosphere. *Journal of Geophysical Research*, 113, Oct 2008.

[27] P. Rannou et al. A new interpretation of scattered light measurements at Titan's limb. *Journal of Geophysical Research: Planets*, 102:10997–11013, May 1997.

[28] M.L. Cable et al. Titan tholins: Simulating Titan organic chemistry in the Cassini-Huygens era. *Chemical Reviews*, 112:1882–1909, Nov 2012.

[29] E.J.L. Larson et al. Simulating Titan's aerosols in a three dimensional general circulation model. *Icarus*, 243:400–419, Nov 2014.

[30] R. Lopes et al. A global geomorphologic map of Saturn's moon Titan. *Nature*, pages 228–233, Nov 2020.

[31] M.J. Malaska et al. Labyrinth terrain on Titan. *Icarus*, 344, Jul 2020.

[32] S.P.D. Birch et al. Geomorphologic mapping of Titan's polar terrains: Constraining surface processes and landscape evolution. *Icarus*, 282:214–236, Jan 2017.

[33] O. Aharonson et al. An asymmetric distribution of lakes on Titan as a possible consequence of orbital forcing. *Nature Geoscience*, pages 851–854, Nov 2009.

[34] J.M. Lora et al. Simulations of Titan's paleoclimate. *Icarus*, 243:264–273, Sep 2014.

[35] S.P.D. Birch et al. Morphological evidence that Titan's southern hemisphere basins are paleoseas. *Icarus*, 310:140–148, 2018.

[36] M.A. Janssen et al. Titan's surface at 2.18-cm wavelength imaged by the Cassini RADAR radiometer: Results and interpretations through the first ten years of observation. *Icarus*, 270:443–459, May 2016.

[37] C.A. Janssen et al. A corridor of exposed ice-rich bedrock across Titan's tropical region. *Nature Astronomy*, pages 642–648, Apr 2019.

[38] M.J. Malaska et al. Geomorphological map of the Afekan Crater region, Titan: Terrain relationships in the equatorial and mid-latitude regions. *Icarus*, 270:130–161, 2005.

[39] J. Radebaugh. *Alluvial and fluvial fans on Saturn's moon Titan reveal processes, materials and regional geology.* Geological Society of London Special Publication, 2016.

[40] A. Hayes et al. Hydrocarbon lakes on Titan: Distribution and interaction with a porous regolith. *Geophysical Research Letters*, 35, May 2008.

[41] J. Radebaugh et al. Linear dunes on Titan and Earth: Initial remote sensing comparisons. *Icarus*, 121:122–132, Sep 2010.

[42] J. Radebaugh, A. Le Gall, R. Lorenz, and J. Lunine. Stabilized dunes on Titan as indicators of climate change. pages 1546–, Oct 2011.

[43] J.W. Barnes et al. Spectroscopy, morphometry, and photoclinometry of Titan's dunefields from Cassini/VIMS. *Icarus*, pages 400–414, 2008.

[44] S. Rodriguez et al. Global mapping and characterization of Titan's dune fields with Cassini: Correlation between RADAR and VIMS observations. *Icarus*, 230:168–179, Nov 2014.

[45] J. Radebaugh et al. Dunes on Titan observed by Cassini Radar. *Icarus*, 194:690–703, Apr 2008.

[46] T. Tokano. Relevance of fast westerlies at equinox for the eastward elongation of Titan's dunes. *Aeolian Research*, pages 113–127, Nov 2010.

[47] B. Charnay et al. Methane storms as a driver of Titan's dune orientation. *Nature Geoscience*, pages 362–366, Apr 2015.

[48] J. Radebaugh et al. Regional geomorphology and history of Titan's Xanadu province. *Icarus*, 211:672–685, Jan 2011.

[49] R.M.C. Lopes et al. Distribution and interplay of geologic processes on Titan from Cassini radar data. *Icarus*, 205:540–558, Feb 2010.

[50] R.D. Lorenz et al. Titan's young surface: Initial impact crater survey by Cassini RADAR and model comparison. *Geophysical Research Letters*, 34, Apr 2007.

[51] L. Wye et al. Electrical properties of Titan's surface from Cassini RADAR scatterometer measurements. *Icarus*, 188:367–385, Jun 2007.

[52] J. Radebaugh et al. Mountains on Titan observed by Cassini Radar. *Icarus*, 192:77–91, Aug 2007.

[53] R. Lopes et al. Cryovolcanism on Titan: New results from Cassini RADAR and VIMS. *Journal of Geophysical Research: Planets*, 118:416–435, Mar 2013.

[54] J.S. Kargel. Cryovolcanism on the Icy Satellites. In Moustafa T. Chahine et al., editors, *Comparative Planetology with an Earth Perspective*, pages 101–113. Springer Netherlands, 1995.

[55] R. Lopes et al. Cryovolcanic features on Titan's surface as revealed by the Cassini Titan Radar Mapper. *Icarus*, 186:395–412, Feb 2007.

[56] C.A. Wood et al. Impact craters on Titan. *Icarus*, 206:334–344, 2010.

[57] J.M. Soderblom et al. Geology of the Selk crater region on Titan from Cassini VIMS observations. *Icarus*, 208:905–912, Aug 2010.

[58] C.D. Neish et al. Spectral properties of Titan's impact craters imply chemical weathering of its surface. *Geophysical Research Letters*, 42:3746–3754, May 2015.

[59] A.G. Hayes et al. A post-Cassini view of Titan's methane-based hydrologic cycle. *Nature Geoscience*, 11:306–313, Apr 2018.

[60] A.G. Hayes. The Lakes and Seas of Titan. *Annual Reviews*, 44:57–83, Jun 2016.

[61] A.G. Hayes et al. Transient surface liquid in Titan's polar regions from Cassini. *Icarus*, 211:655–671, 2011.

[62] J.M. Moore and A.D. Howard. Are the basins of Titan's Hotei Regio and Tui Regio sites of former low latitude seas? *Geophysical Review Letters*, 38, 2011.

[63] A.E. Gilliam and A. Lerman. Titan's missing ethane: From the atmosphere to the subsurface. *Icarus*, 275:252–258, Sep 2016.

[64] J.I. Lunine, D.J. Stevenson, and Y.L. Yung. Ethane ocean on Titan. *Science*, 222:1229–1230, Dec 1983.

[65] A.G. Hayes et al. Topographic constraints on the evolution and connectivity of Titan's lacustrine basins. *Geophysical Research Letters*, 44:11745–11753, Nov 2017.

[66] H.G. Roe. Titan's Methane Weather. *Annual Review of Earch and Planetary Sciences*, 40:355–382, 2012.

[67] R.D. Lorenz et al. Photochemically driven collapse of Titan's atmosphere. *Science*, 275:642–644, Jan 1997.

[68] P.F. Penteado et al. Latitudinal variations in Titan's methane and haze from Cassini VIMS observations. *Icarus*, 206:352–365, Nov 2010.

[69] R.D. Lorenz et al. Titan's inventory of organic surface materials. *Geophysical Research Letters*, 35, Jan 2008.

[70] S.K. Atreya et al. Titan's methane cycle. *Icarus*, 54:1177–1187, Oct 2006.

[71] G. Tobie, D. Gautier, F. Hersant, and J.I. Lunine. *Interpretation of Titan's atmospheric composition measured by Cassini-Huygens*, page 668. Sep 2008.

[72] C. Beghin, C. Sotin, and M. Hamelin. Titan's native ocean revealed beneath some 45 km of ice by a Schumann-like resonance. *Icarus*, 342:425–433, Jun 2010.

[73] L. Iess et al. The tides of Titan. *Science*, 337:457–459, Jul 2012.

[74] S. Wall et al. Active shoreline of Ontario Lacus, Titan: A morphological study of the lake and its surroundings. *Geophysical Research Letters*, 37, Mar 2010.

[75] S.P.D. Birch et al. Alluvial fan morphology, distribution and formation on titan. *Icarus*, 270:238–247, May 2016.

[76] J.M. Moore et al. The landscape of Titan as witness to its climate evolution. *Journal of Geophysical Research: Planets*, 119:2060–2077, Sep 2014.

[77] R.D. Lorenz et al. Fluvial channels on Titan: initial Cassini RADAR observations. *Planetary Space Science*, 56:1132–1144, 2008.

[78] J.I. Lunine and S.K. Atreya. The methane cycle on Titan. *Nature Geoscience*, 1:159–164, Feb 2008.

[79] V. Poggiali et al. Liquid-filled canyons on Titan. *Geophysical Research Letters*, 43:7887–7894, Aug 2016.

[80] R.D. Lorenz. The weather on Titan. *Science*, 290:467–468, Oct 2000.

[81] E. Lellouch et al. The distribution of methane in Titan's stratosphere from Cassini/CIRS observations. *Icarus*, 231:323–337, Mar 2014.

[82] R.D. Lorenz et al. A radar map of Titan seas: tidal dissipation and ocean mixing through the throat of Kraken. *Icarus*, 237:9–15, 2014.

[83] R.D. Lorenz and A.G. Hayes. The growth of wind-waves in Titan's hydrocarbon seas. *Icarus*, 219:468–475, 2012.

[84] J.L. Mitchell and J.M. Lora. The Climate of Titan. *Annual Review of Earth and Planetary Sciences*, 44:53–80, 2016.

[85] R.D. Lorenz et al. Titan's damp ground: Constraints on Titan surface thermal properties from the temperature evolution of the Huygens GCMS inlet. *Meteoritics and Planetary Science*, 41:1705–1714, Nov 2006.

[86] C.A. Griffith et al. Detection of daily clouds on Titan. *Science*, 290:509–513, 2000.

[87] M.E. Brown et al. Direct detection of variable tropospheric clouds near Titan's south pole. *Nature*, 420:795–797, 2002.

[88] F. Hourdin et al. Numerical Simulation of the General Circulation of the Atmosphere of Titan. *Icarus*, 117:358–374, Oct 1995.

[89] J.M. Lora and J.L. Mitchell. Titan's asymmetric lake distribution mediated by methane transport due to atmospheric eddies. *Geophysical Research Letters*, 42:6213–6220, 2015.

[90] T. Scheider et al. Polar methane accumulation and rainstorms on Titan from simulations of the methane cycle. *Nature*, 481:58–61, 2012.

[91] J.M. Lora et al. GCM simulations of Titan's middle and lower atmosphere and comparison to observations. *Icarus*, 250:516–528, Apr 2015.

[92] C.R. Mechoso and A. Arakawa. *Numerical Models: General Circulation Models*, pages 153–160. Academic Press, second edition, 2015.

[93] S. Collins et al. *Grids in Numerical Weather and Climate Models*, pages 111–126. 2013.

[94] T. Tokano. Orbitally and geographically caused seasonal asymmetry in Titan's tropospheric climate and its implication for the lake distribution. *Icarus*, 317:337–353, 2019.

[95] J.M. Lora and M. Ádámkovics. The near-surface methane humidity on Titan. *Icarus*, 286:270–279, Oct 2017.

[96] I.M. Held. The Partitioning of Poleward Energy Transport Between the Tropical Ocean and Atmosphere. *Journal of the Atmospheric Science*, 58:948–953, Apr 2001.

[97] N. Siler et al. Insights into the Zonal-Mean Response of the Hydrologic Cycle to GlobalWarming from a Diffusive Energy Balance Model. *Journal of Climate*, 31:7481–7493, Sep 2018.

[98] D. Bolton. The Computation of Equivalent Potential Temperature. *Monthly Weather Review*, 108:1046–1053, Jul 2018.

[99] D.M. Williams and J.F. Kasting. Habitable Planets with High Obliquities. *Icarus*, 129:254–267, Apr 1997.